DOCTORAL DISSERTATION

Study on permafrost and ground surface conditions at the Taiga-Tundra boundary in the Indigirka River lowland, northeastern Siberia

北東シベリアインディギルカ河川低地タイガ-ツンドラ境界

における永久凍土と地表面状態に関する研究

Division of Earth System Science,

Graduate School of Environmental Science,

Hokkaido University

北海道大学大学院環境科学院地球圏科学専攻

Shinya TAKANO

鷹野　真也

February 2020

Abstract

There seems to be an interaction between permafrost and the ground surface conditions such as vegetation, microtopography, and snow cover in Arctic region. In this study, we conducted (1) investigation of a relationship between the ground ice and the vegetation/microtopography, and also the ground ice formation conditions, and (2) snow survey to observe the spatial distribution of snow cover, at the Taiga–Tundra boundary near Chokurdakh (70°37′N, 147°53′E) in the Indigirka River lowlands of northeastern Siberia. The stable isotopic composition of water ($\delta^{18}O$, δD, and d-excess) was used to estimate the source and freezing rate of ground ice and sublimation and re-distribution processes of snow cover.

The gravimetric water content (GWC) in the frozen soil layer was significantly higher at microtopographically high elevations with growing larch trees (i.e., tree mounds) than at low elevations with wetland vegetation (i.e., wet areas). The observed ground ice (ice-rich layer) with a high GWC in the tree mounds suggests that the relatively elevated microtopography of the land surface, which was formed by frost heave, strongly affects vegetation composition. Large variations in the isotope ratios of the ground ice ($\delta^{18}O$ was from –25.7‰ to –21.8‰) were observed for the ice-rich layer with high ice content in the tree mounds. The slope of the regression line of these data in the δD–$\delta^{18}O$

plot was 6.9, suggesting a near equilibrium isotope fractionation occurred during freezing. This implies that the ice formed with sufficient time for the migration of unfrozen soil water to the freezing front (i.e., ice segregation), therefore thick ice lenses formed. In contrast, narrow variation range in the isotopic data ($\delta^{18}O$ was from –22.4‰ to –20.4‰) with low ice content of approximately 130% was observed in the wet areas. It was indicated that rapid freezing occurred under relatively non-equilibrium conditions, implying that there was insufficient time for ice segregation to occur.

The freezing rate of the tree mounds was slower than that of the wet areas due to the difference of such as soil moisture and snow cover which control underground thermal conductivity. A clear relationship between the snow cover parameters and the vegetation was observed in the study area. Snow cover was the deepest at the site covered by dense and tall shrub (69 cm in 2014 and 60 cm in 2015), while snow density was the highest on ice over a lake (0.277 g/cm^3 in 2014 and 0.227 g/cm^3 in 2015). The Snow water equivalent (SWE) was the highest at the shrub site (135 mm in 2014 and 113 mm in 2015), whereas that was the lowest at the site of sedge and/or sphagnum wetland (84 mm in 2014 and 66 mm in 2015). Since the clear relationship between SWE and vegetation type, we estimated regional SWE in observation area (10 × 10 km) using a vegetation map. The values were 111 mm in 2014 and 86 mm in 2015.

It was shown that there is an interaction between permafrost and ground surface conditions in this study area. The warming and increase in snowfall predicted in the future will affect degradation of the permafrost, which can have a significant impact on the microtopography and the vegetation structure and composition. In addition, the current increases in trees and shrubs in the Taiga–Tundra boundary greatly contributes to the distribution in snow cover on a regional scale, which may suppresses the ground temperature cooling in winter. Future climate change will have a significant impact on the freezing environment of ground ice and change the ground surface conditions, then they may interact further.

Keywords: Stable isotopes of water, ground ice, ice content, permafrost, microtopography, snow cover, snow depth, snow water equivalent, Taiga-Tundra-boundary, Siberia, Arctic

Contents

Chapter 1. General introduction

1.1. Global warming and Taig‒Tundra boundary on permafrost

During the past century, global temperatures increased and larger warming trend has been observed in Arctic regions (e.g., IPCC SR, 2018; Serreze and Barry, 2011). The trend in the high-latitude areas are expected to continue for the next 100 years (IPCC AR5 WG1, 2013).

Along with the increase in the air temperature, warming trend of ground temperature has been observed in permafrost area since the 1980s (IPCC AR5 WG1, 2013). In Siberia, an increase in ground temperature (0 cm depth) of approximately 0.5-2 °C has been observed since the 1970s (Romanovsky et al., 2007; 2010). It has been reported that the increase rate of ground temperature in Eastern Siberia was 0.22 °C /10 years, which was particularly large (Romanovsky et al., 2007; Park et al., 2014). Park et al. (2014) reported that the increase rate of ground temperature was larger than that of air temperature in Siberia, suggesting it was due to an amplified impact of snow depth.

Numerical models have calculated an increase in snowfall and snow water equivalent (SWE) in the Arctic region, especially in northeastern Siberia, in the second half of the 21st century (e.g. Raisanen, 2008; Callaghan, 2011; Bring et al., 2016). This increase in snow cover greatly affects soil freezing environment, such as disturbance of ground temperature cooling in winter. Therefore, the increase in snow cover and air temperature will have a major impact on the permafrost area, and changes in the soil freezing environment need to be considered.

Permafrost zones occupy approximately 24% (22.79 million km^2) of the land area in the Northern Hemisphere (Zhang et al., 2003) and Taiga–Tundra boundary covers over 1.9 million km^2 of the circum-Arctic region (Ranson et al., 2011). Vast Taiga forests and Tundra wetlands on the permafrost play an important role in the global carbon cycle as carbon sinks and/or CH_4 sources (McGuire et al., 2009).

In this area, changes in vegetation and microtopography are recently reported. Thermokarst processes in the permafrost caused waterlogging and vegetation change from forest to wetland (e.g. Jorgenson et al., 2001). In addition, NDVI (Normalized Difference Vegetation Index), trees and shrubs are currently increasing (Kravtsova and Loshkareva, 2013; Frost and Epstein, 2014).

1.2. Permafrost and ground surface conditions (vegetation, microtopography, and snow cover)

Ground ice is part of the permafrost and can control the vegetation structure and composition in the Arctic permafrost zone. In the Arctic tundra, polygon mires are a typical microtopographic landscape (Boch, 1974) and cover approximately 250,000 km^2 of the circum-Arctic region (Minke et al., 2007). They are formed by the growth of ground ice such as ice wedges (Chernov and Matveyeva, 1997), and a clear zonation of vegetation has been observed corresponding to the polygonal pattern in the microtopography (Minke et al., 2009; Wolter et al., 2016; Zibulski et al., 2016). This means that ground ice forms a ridge (i.e., relatively high ground surface and high frost table) that causes relatively dry soil conditions (Boudreau and Rouse, 1995; Engstrom et al., 2005; Godin et al., 2016); thus, it controls the vegetation structure and composition in the Arctic tundra area.

Snow accumulation patterns at the regional scale in the tundra are controlled by not only difference in precipitation but also by the complex interaction of blowing snow (re-distribution) with vegetation and microtopography (e.g. Essery and Pomeroy, 2004; Hirashima et al., 2004; Rees et al., 2014), and sublimation (25-50% of total snowfall) (e.g. Pomeroy et al., 1997, 1998; Liston and Sturm, 1998; Essery et al., 1999; Pomeroy and Essery, 1999). The snow cover suppresses the ground temperature cooling in winter as an insulator (e.g. Zhang, 2005), so the spatial variation in the snow cover will cause that in the ground temperature at the regional scale.

1.3. Stable isotopes of water

Stable isotope ratios of water are a useful tool (e.g., Stuiver et al., 1976; Mackey, 1983) for determining source water and have long been utilized in studies on the water cycle (e.g., Craig, 1961; Dansgaard, 1964; Craig and Gordon, 1965). The isotopic compositions were expressed in delta notation relative to Vienna Standard Mean Ocean Water (VSMOW). The delta values were defined as follows:

$$\delta^{18}O \ or \ \delta D = \{(R_{sample} - R_{VSMOW})/R_{VSMOW}\} \times 1000 \ (‰), \tag{1}$$

where R_{sample} and R_{VSMOW} are the water isotopic ratios ($^{18}O/^{16}O$ or D/H) of the samples and VSMOW, respectively. Deuterium excess (d-excess), which is an indicator of non-equilibrium processes (e.g., Craig and Gordon, 1965; Merlivat and Jouzel, 1979), was calculated from $\delta^{18}O$ and δD as follows (Dansgaard, 1964):

$$d\text{-}excess = \delta D - 8 \times \delta^{18}O. \tag{2}$$

The d-excess and the regression slope between $\delta^{18}O$ and δD can be used as an indicator for the equilibrium or non-equilibrium state during such as the evaporation process (e.g., Craig and Gordon, 1965; Merlivat and Jouzel, 1979) and the freezing process (Suzuoki and Kimura, 1973; Lacelle, 2011; O'Neil, 1968). The water isotope ratios of the ice provide some information about the freezing environment during ground ice formation (e.g., Suzuoki and Kimura, 1973; Lacelle, 2011; Michel, 2011), as has been observed in northern Siberia (Meyer et al., 2002a; 2002b; 2015; Opel et al., 2011; 2017;

Wetterich et al., 2011; 2014; 2016; Iwahana et al., 2014; Vasil'chuk and Vasil'chuk, 2014; Streletskaya et al., 2015) and other Arctic and sub-Arctic regions (Meyer et al., 2010; Fritz et al., 2012; Yoshikawa et al., 2012; 2013; Lachniet et al., 2012; Porter et al., 2016; Schirrmeister et al., 2016). The $\delta^{18}O$ values of the ice have been reported to be enriched by 2.8–3.1‰ compared to the source water when frozen under isotopically equilibrium conditions (Suzuoki and Kimura, 1973; O'Neil, 1968), and the delta values gradual decreased from the first formed ice to the subsequent ices according to Rayleigh-type isotope fractionation (S1 Appendix). In the $\delta D-\delta^{18}O$ plot, the slope of the regression line of the isotopic compositions of ice formed during the equilibrium freezing shows from approximately 6 to 7.3, and that formed under the non-equilibrium freezing shows lower values (Suzuoki and Kimura, 1973; Lacelle, 2011).

1.4. Research aim

Here, we face two main research questions as follow:

(1) How is the relationship among permafrost, vegetation, microtopography, and snow cover in Taiga–Tundra boundary?

(2) How the ground surface conditions affect soil freezing environment in Taiga–Tundra boundary?

The purpose of this study is set to examine the possible responses of the ground ice, microtopography, and vegetation structure and composition in the Arctic Taiga–Tundra boundary for future climate change. In this study, I assessed a relationship between the ground ice and the vegetation/microtopography, and also the ground ice formation conditions (e.g., source of ice, freezing rate) at the Taiga–Tundra boundary near Chokurdakh in the Indigirka River lowlands of northeastern Siberia (Chapter 3). I also conducted snow survey to observe the spatial distribution of snow cover and calculate local Snow Water Equivalent (SWE) in the area (Chapter 4).

Chapter 2. Methods

2.1. Study area

We selected four observation sites with different densities of larch trees (from least to highest): Boydom (site B), Kodac (site K), Allikha (site A) and Verkhniy Khatistakh (site V). These sites are near Chokurdakh (70°37′N, 147°53′E), which is downstream of the Indigirka River in northeastern Siberia (Fig 2.1 and Table 2.1). All field studies were organized by the Institute for Biological Problems of Cryolithozone, Siberian Branch of the Russian Academy of Sciences, Yakutsk, Sakha, Russia with permissions from Federal Service for Technical and Export Control. The mean annual air temperature is −13.9 °C, and the mean monthly air temperatures in January and July are −34.2 and 10.0 °C, respectively. The annual mean precipitation at Chokurdakh from 1950–2008 was 210 mm according to the Baseline Meteorological Data in Siberia (BMDS) Version 5.0 (Yabuki et al., 2011). Summer temperatures during the past 50 years have shown a warming trend, winter precipitation during the past century showed an increase trend (Vaganov et al., 1999; Tei et al., 2017). In recent years, larch and tall shrub coverage has increased (Frost and Epstein, 2014), and an increase in invasive (expanded) plant species from more southerly regions has been reported (Khitun et al., 2016).

This observation area is underlain by continuous permafrost. Normally, snowmelt and active layer thawing start in the late May through to early June; the growing season is from late June to early August. The average thaw depth observed between 3 July and 9 August at the study sites was 31±12 cm (Shingubara et al., 2019), whereas the maximum thaw depth was found at the end of thaw season (the first half of September). The active layer begins to freeze in the second half of September through to October and freezes completely between November and December.

The observation area is located on the Taiga–Tundra boundary. This area has mound-shaped landforms and wetlands distributed in patches. These mounds look like palsa or peat plateaus and were named "tree mounds" in this study. The vegetation on tree mounds is mainly larches (*Larix cajanderi, syn. L. gmelinii*), shrubs (including *Betula nana* and *Salix spp.*) and green-mosses (including *Tomentypnum nitens*, *Hylocomium splendens*, and *Aulacomnium turgidum*). Wetlands were labeled as "wet areas" in this study; their vegetation includes sedges (*Eriophorum spp.* and *Carex spp.*) and sphagnum-mosses (including *Sphagnum balticum, S. squarrosum, S. angustifolium*). The transitional area between tree mounds and wet areas contained shrubs with sphagnum-mosses and was labeled as "intermediate areas". Detailed data were obtained on the vegetation, which as classified into several classes (including tree, shrub, willow, cotton-sedge, and *Sphagnum*) based on plant species identified by Morozumi et al. (2019). In this study, the tree, shrub, and willow classes were grouped into tree mounds, and the cotton-sedge and *Sphagnum* classes were grouped into wet areas.

Among the four sites, site B was close to a tundra landscape with several larch trees on an isolated tree mound. Site K (Fig 2.2) was typical Taiga–Tundra boundary ecosystem. Larch trees grew on tree mounds, while many dead larches were observed in wet areas. Site A was at the foot of a hill with a peak of approximately 40–60 m above the river level. Larch trees grew on the slope of the hill, and steppe tundra covered the top with few or no larch trees. Site V was a relatively dense larch forest in a narrow area along the mainstream of the Indigirka River. Riparian areas were covered by willows and alders. The vegetation at these sites was also described by Liang et al. (2014) and Fan et al. (2018).

2.2. Water isotope analysis

The water samples were analyzed for the stable isotopic composition of water (oxygen and hydrogen) with the $CO_2/H_2/H_2O$ equilibration method using a mass spectrometer (MAT 253, Thermo Fisher Scientific, USA, manufactured in Germany) attached to a Gas Bench (Thermo Fisher Scientific, USA, manufactured in Germany) at the Graduate School of Environmental Science, Hokkaido University, Japan. The precision of the analysis was within ±0.2‰ for $\delta^{18}O$ and ±2‰ for δD.

In this research, we used the observed $\delta^{18}O$ and δD values and d-excess. We also used the slope of δD–$\delta^{18}O$ plot to understand the equilibrium and non-equilibrium fractionations (Lacelle, 2011; Kendall and McDonnell, 1998). During the freezing process, when equilibrium fractionation occurs, the slope of δD–$\delta^{18}O$ plot shows from approximately 6 to 7.3 at 0 °C. Non-equilibrium fractionation shows lower slope of δD–$\delta^{18}O$ plot, and when no fractionation occurs, isotopic composition of formed ice is the same composition as water $\delta^{18}O$ and δD. An intercept of δD–$\delta^{18}O$ plot is different from d-excess. We did not use the intercept of δD–$\delta^{18}O$ plot in this research, and the d-excess value was defined as described in the equation (2).

Table 2.1. Summary of the observation and sampling data.

Site	Latitude Longitude	Sampling point	Sampling date	Sampling depth (cm)	Thaw depth (cm)	Landscape & vegetation category	Profile pattern
B	70° 38'15"N 148° 09'17"E	B1	9 July 2011	90	20	Tree mound	i
		B2	9 July 2011	90	30	Wet area	i
		B3	20 July 2012	103	26	Tree mound	i
		B4	20 July 2012	92	40	Wet area	i
K	70° 33'48"N 148° 15'51"E	K1	10 July 2011	90	20	Tree mound	i, ii
		K2	10 July 2011	90	20	Tree mound	i, iii
		K3	10 July 2011	90	30	Wet area	iv
		K4	11 July 2011	90	20	Tree mound	i, iii
		K5	11 July 2011	90	20	Tree mound	i
		K6	11 July 2011	90	20	Intermediate	i
		K7	16 July 2012	100	50	Tree mound	ii
		K8	17 July 2012	98	13	Tree mound	ii
		K9	19 July 2012	99	20	Tree mound	ii
		K10	19 July 2012	97	30	Wet area	iv
		K11	19 July 2012	104	33	Wet area	iv
		K12	20 July 2012	102	30	Intermediate	iv
V	70° 15'07"N 147° 28'08"E	V1	23 July 2011	90	20	Tree mound	i
		V2	23 July 2011	90	30	Wet area	i
		V3	26 July 2012	98	42	Tree mound	anomaly
		V4	26 July 2012	94	40	Wet area	iv
A	70° 30'56"N 147° 18'15"E	A1	24 July 2011	90	40	The slope of a hill	i
		A2	24 July 2011	90	20	Intermediate	iv

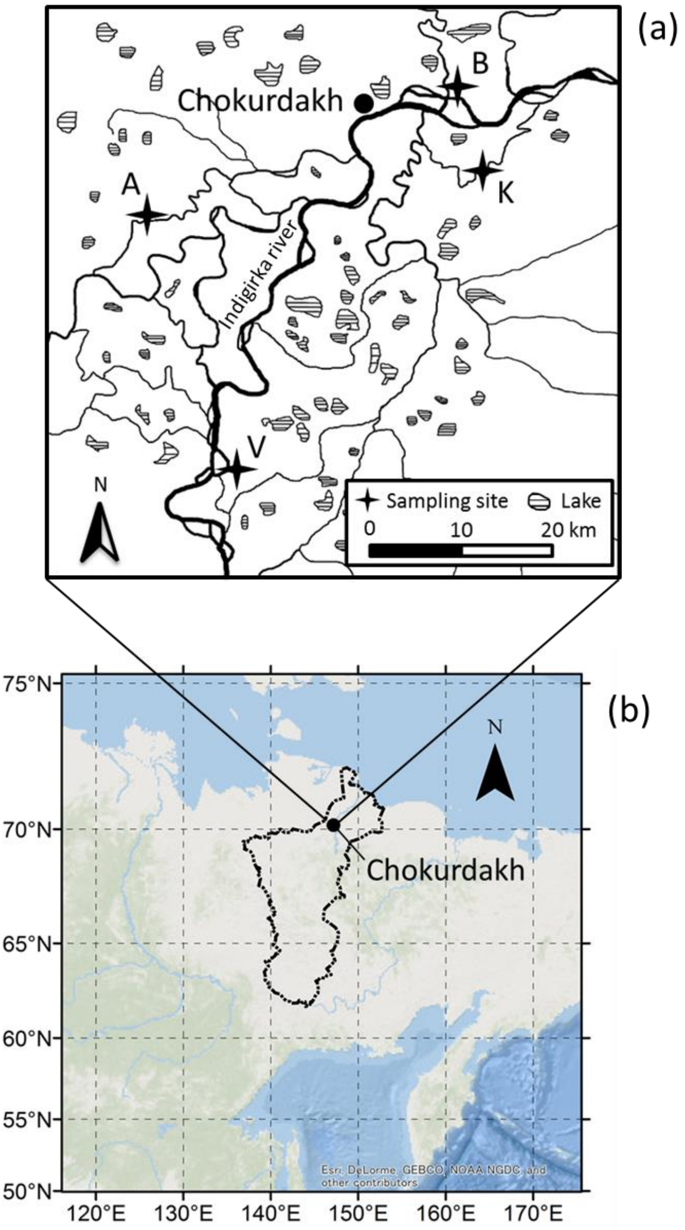

Fig 2.1. Locations of the study sites in northeastern Siberia. (a) Thick and thin lines represent the Indigirka River and its tributaries, respectively, and the filled areas are lakes. Chokurdakh village and other observation sites V, A, K, and B are also indicated, modified by Liang et al. (2014). (b) The Indigirka River basin is shown with a line.

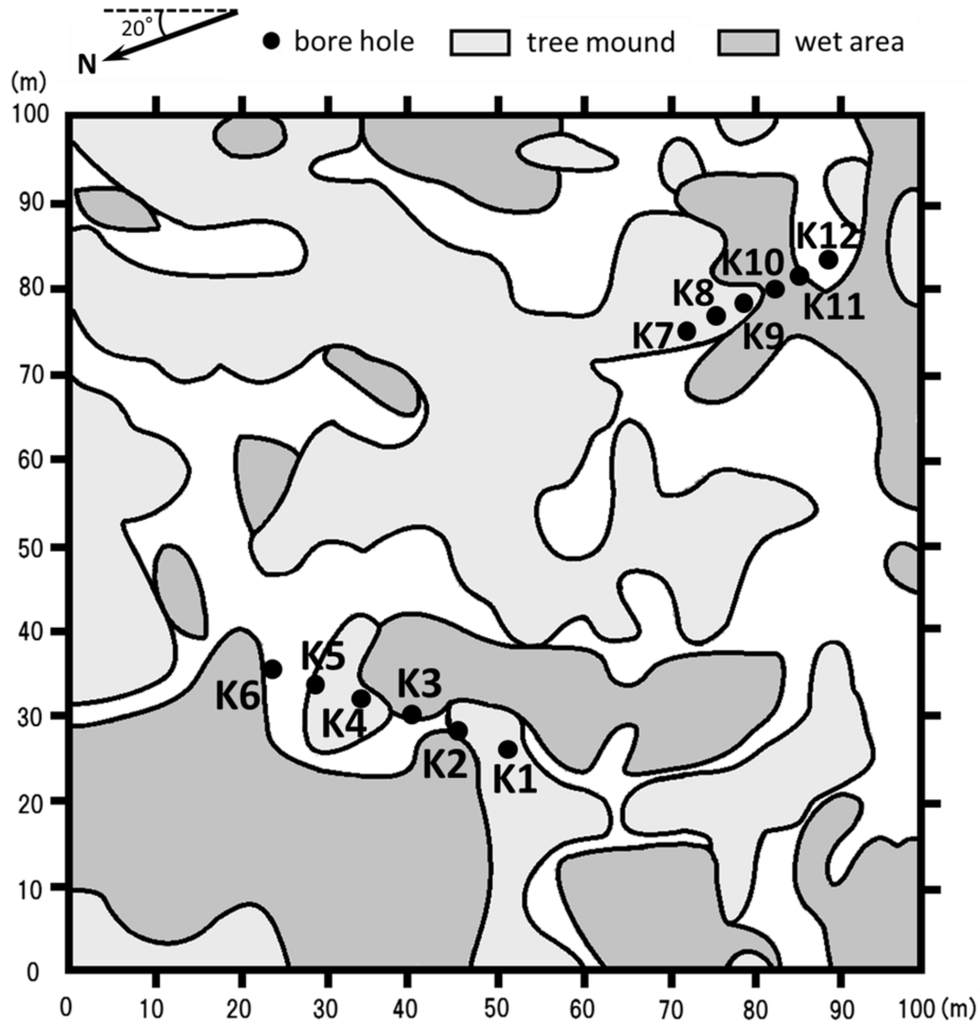

Fig 2.2. Map of the observation plot at site K. Landscape/vegetation is shown as patterns. Light, thick shaded, and open patterns indicate tree mounds, wet areas, and intermediate areas, respectively. Closed circles represent boreholes from which the frozen soil cores were obtained. Modified by Liang et al. (2014).

Chapter 3. Isotopic compositions of ground ice in near-surface permafrost in relation to vegetation and microtopography at the Taiga–Tundra boundary in the Indigirka River lowlands, northeastern Siberia

3.1. Introduction

Permafrost zones occupy approximately 24% (22.79 million km^2) of the land area in the Northern Hemisphere (Zhang et al., 2003). Taiga and Tundra ecosystems are located on the permafrost and play an important role in the global carbon cycle as carbon sinks and/or CH_4 sources (McGuire et al., 2009). The warming trend in high-latitude areas caused by Arctic amplification (e.g., Serreze and Barry, 2011) is expected to lead to drastic changes such as permafrost degradation (e.g., Lemke et al., 2007), forest productivity changes (e.g., Tei et al., 2017; Tei and Sugimoto, 2018), and tree line shifts (e.g., Tchebakova et al., 2009; Frost and Epstein, 2014). Therefore, it is necessary to understand how permafrost and vegetation respond to climate change in high-latitude areas.

The Taiga–Tundra boundary covers over 1.9 million km^2 of the circum-Arctic region (Ranson et al., 2011) and is expanding because trees and shrubs are currently increasing in tundra ecosystems (Frost and Epstein, 2014; Kravtsova and Loshkareva, 2013). In addition, thermokarst processes in the permafrost change the vegetation from forest to wetland at this boundary (e.g., Jorgenson et al., 2001), which may cause CH_4 emissions.

Ground ice is part of the permafrost and can control the vegetation structure and composition. In the Arctic tundra, polygon mires are a typical microtopographic landscape (Boch, 1974) and cover approximately 250,000 km^2 of the circum-Arctic region (Minke et al., 2007). They are formed by the growth of ground ice such as ice wedges (Chernov and Matveyeva, 1997), and a clear zonation of vegetation has been observed corresponding to the polygonal pattern in the microtopography (Minke et al., 2009; Wolter et al., 2016; Zibulski et al., 2016). This means that ground ice forms a ridge (i.e., relatively high ground surface and high frost table) that causes relatively dry soil conditions (Boudreau and Rouse, 1995; Engstrom et al., 2005; Godin et al., 2016); thus, it controls the vegetation structure and composition in the Arctic tundra area. Although polygon mires are mainly covered by wetland vegetation, the microtopographic landscape may also affect the vegetation structure and composition in the Taiga–Tundra boundary ecosystem. It has been reported that near-surface ground ice characteristics are closely related to vegetation type owing to physical conditions associated with differences in the alluvial environments of Arctic Canada (Kokelj and Burn, 2005), and there are many other studies on ground ice content in relation to vegetation and microtopography (e.g., Kokelj and Burn, 2003; Kokelj et al., 2007; Burn and Kokelj, 2009; Morse and Burn, 2013).

The ground ice (e.g., ice wedges and segregation ice (Van Everdingen, 1998)) in permafrost is generally formed by the infiltration of water, which is kept in the soil and freezes. Ice segregation frequently occurs in the transition zone, which is at the uppermost layer of the permafrost and alternates between an active layer and permafrost over periods ranging from less than a decade to multiple centuries (Shur et al., 2005; French and Shur, 2010). The transition zone experiences favorable thermal and hydrological conditions for ice segregation, such as water saturation and slow freezing, and frequently forms ice lenses parallel to the ground surface with high ice content (S1 Appendix).

The freezing rate is one of the most important factors for ground ice formation in soil. Slow freezing can provide sufficient time for unfrozen soil water to slowly migrate to the freezing front (S1 Appendix). The freezing rate depends on the thermal conductivity in the surface soil, which fluctuates due to such as soil moisture, soil type, snow cover, and vegetation (Matsumoto and Ohkubo, 1977; Hinzman et al., 1991; Zhang, 2005). The thermal conductivity (i.e., the freezing rate) increases when higher soil moisture, less organic layer, and less snow cover, and inversely decreases when lower soil moisture, more organic layer, and more snow cover. Therefore, the freezing rate can be affected by these factors.

Iwahana et al. (2014) observed the current thermal regime of the active layer and spatial variations in the ice content, soil mechanical characteristics, cryostratigraphy, and water stable isotope ratio of near-surface permafrost in the Indigirka River lowlands of northeastern Siberia. They found similarities in the geocryological characteristics in the research area, which suggests that the formation of the upper 1 m cryostratigraphy may have been affected by similar hydrological conditions in the area.

For better understanding of the possible responses of the ground ice, microtopography, and vegetation structure and composition in the Arctic Taiga–Tundra boundary to future climate change, it is necessary to assess the ground ice formation conditions and how ground ice is related to the vegetation and microtopography. Therefore, we examined the ice content and isotopic compositions of near-surface permafrost down to a depth of 1 m at the Taiga–Tundra boundary near Chokurdakh in the Indigirka River lowlands of northeastern Siberia.

3.2. Methods

3.2.1. Observation and samplings

Observation (vegetation structure and composition and microtopography) and sampling (soil and soil water) data were collected at each site, especially for site K, in the periods of 9–24 July 2011 and 16–26 July 2012. The data are summarized in Table 2.1.

Transects and soil sampling

Frozen soil cores down to a depth of approximately 1 m were obtained at all sites with a boring machine (power auger; Tanaka TIA-350S, Nikko Tanaka Engineering Co., Ltd., Chiba, Japan). Core samples with a diameter of approximately 5.5 cm were sampled at intervals of less than 10 cm. Approximately 1 mm was carefully removed from the surface of each sample in order to avoid contamination. Then, each sample was put into a plastic bag. Soil samples of the thaw layer were obtained with a hand shovel and stored similarly as the frozen samples. The organic layer depth and thaw depth were recorded at the same time. At site K, a 30 m transect was set northeast across microtopography and vegetation types and sampled at intervals of 6 m at six points (Points K1–K6 in Fig 2.2) in 2011. Similarly, a 15 m transect was set south and sampled at intervals of 3 m at six points (Points K7–K12 in Fig 2.2) in 2012.

Characteristics of soil grain size distribution in the near-surface ground at the study sites were reported by Iwahana et al. (2014). At site K, soils gradually changed from clay loam to silty clay loam downward. Soils showed small variations in loam or silt loam with depth at site B. Soils at site V varied between loam and clay loam with the largest proportion of sand among the sites. Spatially there was no significant difference in soil texture.

Vegetation and microtopography

Leveling was conducted along the transect sampling points in the observation plot at site K (Fig 2.2) with leveling equipment (automatic level; TOPCON AT-B4, Topcon Corporation, Tokyo, Japan) to determine the relative elevations (microtopography) based on the lowest point (0 cm) along the transects. The vegetation composition and landscape were investigated at each sampling point and categorized into three types: tree mounds, wet areas, and intermediate areas (Table 2.1).

Water extraction and measurements of ice/water content

Water in the soil samples of the thaw layer was taken for isotope analysis and stored in glass vials. Soon after thawing of the frozen core samples in the plastic bags, the water (ice) in the samples was taken and stored similarly. The water was directly taken as a supernatant when the ice/water content of the soil samples was high enough. When the ice/water content was low, water was extracted with a centrifuge.

The weight of the soil samples was measured before and after drying to determine the gravimetric water or ice content. The gravimetric water content (GWC) was calculated as follows (Van Everdingen, 1998):

$$GWC\ (\%) = \left(\frac{Weight\ of\ water\ and\ ice\ in\ the\ sample\ (g)}{Dry\ weight\ of\ the\ sample\ (g)}\right) \times 100. \qquad (3)$$

River water, precipitation, and snow cover sampling

For isotope analysis, river water from the Indigirka mainstream and tributaries was sampled at 14–30 July 2011 and 25 June–11 August 2012. Precipitation was sampled at 29 June–5 August 2012 during the summer. Because of missing observation data for the precipitation during the 2011 summer sampling period, we also sampled precipitation at 23 June–23 July 2013 and 2–19 July 2014 to identify the approximate water isotopic values of summer precipitation. Snow cover was obtained at 23–26 April 2014 and 15–17 April 2015. The bulk snow was obtained as a core with a diameter of 10 cm and put into a plastic bag to melt. The water of the river, precipitation, and snow cover was kept in glass vials.

3.2.2. Statistical analysis

Mann-Whitney U-tests were conducted to examine differences in the values between the tree mounds and wet areas.

3.3. Results

3.3.1. Characteristics of permafrost with different vegetation

Fig 3.1 shows the relative elevations (microtopography) of each sampling point along the two transects at site K. The difference between the lowest and highest points in this sampling area was approximately 50 cm. The averaged relative elevations of the tree mounds and wet areas in site K were 46.4±11.3 cm and 13.7±14.2 cm (Table 3.1), respectively. Thus, the tree mounds had a higher elevation than the wet areas ($p < 0.05$). Fig 3.2 illustrates the microtopography and vegetation composition along the transect sampling points. The understory vegetation of the tree mounds was mainly green-moss, larch, and shrubs (dwarf willow and dwarf birch). That of the wet area was mainly sedge and sphagnum-moss. The average values for the thaw depth, organic layer depth, GWC of the frozen layer, isotopic parameters, relative elevation, and soil density for the samples obtained from the tree mounds and wet areas are given in Table 3.1. The data obtained from the intermediate area are included with the data from the wet areas.

Surface organic layer

A surface organic layer was observed for all samples (Fig 3.3 and S1–S4 Figs). The average depths in the tree mounds and wet areas were 31.6±24.0 cm and 26.9±8.6 cm, respectively, for all sites. No statistical difference was observed (Table 3.1).

Thaw depth

Thaw depth of the wet areas (28.6±5.0 cm) tended to be greater than that of the tree mounds (18.8±2.9 cm) at site K (Table 3.1). A similar tendency was observed at sites A, B, and V. The mean thaw depths of the tree mounds and wet areas were 19.9±3.3 cm and 30.3±6.7 cm, respectively, for all observation sites (Table 3.1). The soil moisture of the thaw layer in wet areas (around 50% in volumetric water content) was generally higher than that in tree mounds (around 20% or less in volumetric water content) (Liang et al., 2014; Shingubara et al., 2019; Morozumi et al., 2019).

Thaw depth usually reaches a maximum during the first half of September, and the maximum depth is considered to be more than 50 cm based on the data of the seasonal variation in ground temperature (S5 and S6 Figs). Although it appears that the observed ground temperature at 75 cm depth slightly exceeded 0 °C, the ground temperature may be artificially high owing to soil disturbance by probe installation.

Water and ice contents

The averaged GWCs of the frozen cores from the tree mounds and wet areas were 167.3±71.1% and 92.6±20.0%, respectively, for all sites. Those at site K were 206.3±58.9% and 100.6±19.5%, respectively (Table 3.1). There were significant differences between the vegetation types at all sites ($p < 0.01$) and at site K ($p < 0.01$).

Most of the frozen cores contained excess ice including numerous ice lenses of various thicknesses. Layers with a high ice content of more than 200% were only observed in the tree mounds of site K and other sites, especially at the top of the frozen layer and at the around 60 cm depth or deeper (Fig 3.3 and S1–S4 Figs). Ice lenses and an ice-rich layer were frequently observed in the frozen layer of the tree mounds but were not common in the wet areas. Consequently, the ice content of the tree mounds often varied with depth, whereas the wet areas showed relatively little variation in the ice content.

Stable isotopic composition of water

The average $\delta^{18}O$ values of ice for the frozen layer in the tree mounds and wet areas were −21.9±0.8‰ and −21.6±0.3‰, respectively, for all sites. No significant difference was observed (Table 3.1). Those for site K were −21.9±1.0‰ and −21.5±0.2‰, respectively, and no significant difference was observed.

The average d-excess values for the frozen layer in the tree mounds and wet areas were 8.1±1.9‰ and 5.4±3.4‰, respectively, for all sites. Those for site K were 7.2±1.8‰ and 3.6±2.5‰, respectively. Significant differences were observed in the data at all sites, and also in that at site K (Table 3.1) using the statistical test. However, since the standard deviation of the average d-excess values were less than the precision of d-excess, there may be differences but not significant differences.

3.3.2. Vertical profiles of the water content, water isotopic ratio, and d-excess

As described above, the tree mounds and wet areas were distinguished by the GWC. We used the $\delta^{18}O$ and δD values to identify four characteristic vertical profiles. Fig 3.3 shows the examples of (i) B3, (ii) K7, (iii) K4, and (iv) K10, and the characteristics of their patterns are described below:

(i) The delta values decreased as the depth of the frozen layer increased.

(ii) The water isotopic ratios showed a different trend in ice-rich layers relative to other layers.

(iii) Low delta and high d-excess values were observed at the bottom of the thaw layer and top of the frozen layer.

(iv) The delta values had a narrow fluctuation range.

Pattern (i)

The B3 sample showed a gradual decrease in the delta values from the surface of the frozen layer (33 cm depth) to the bottom of the core (95 cm depth), as shown in Fig 3.3. $\delta^{18}O$ decreased from −19.5‰ to −24.1‰ (Fig 3.3b), and δD decreased from −146‰ to −185‰ (Fig 3.3c). This pattern was observed in most samples (B1, B2, B3, B4, K1, K2, K4, K5, K6, V1, V2, and A1) except for some samples taken from the wet areas (Table 2.1).

Pattern (ii)

Sample K7 (Fig 3.3e) showed a high ice content (more than 200%) because of the many ice-rich layers (S7 Fig). $\delta^{18}O$ and δD decreased (from −25.4‰ to −24.7‰ and from −193‰ to −188‰, respectively) at a depth of approximately 70–80 cm compared to in the adjacent upper and lower ice-rich layers (Figs 3.3f and g). Ice-rich layers were also observed in samples K1, K8, and K9, and their delta values showed different trends relative to other layers (S1 and S2 Figs). All samples categorized in pattern (ii) were observed in the tree mounds (Table 2.1).

Pattern (iii)

The thaw layer at K4 showed a higher water content and d-excess (388.6% and 15‰, respectively) at a depth of 15 cm than at 5 cm (220.0% and 4‰, respectively) (Figs 3.3i and l). On the other hand, the delta values at the 15 cm depth were clearly lower ($\delta^{18}O$ = −24.1‰, δD = −177‰) than those of the other layers (Figs 3.3j and k). The surface frozen layer in sample K4, which had large amounts of pure ice (S7 Fig), had a higher ice content (550.6%) than the below layer (Fig 3.3i). The delta values of the layer ($\delta^{18}O$ = −22.0‰, δD = −166‰) were lower than those of the layer below (Figs 3.3j and k), but d-excess (11‰) was higher (Fig 3.3l). We found this pattern in a number of 2011 site K cores obtained from tree mounds that had cracks on the surface (Table 2.1).

Pattern (iv)

The ice content of the frozen layer at K10, which was obtained from a wet area (Table 2.1), was low at approximately 120%, and the variation range was narrow (Fig 3.3m). Furthermore, there was no ice-rich layer (S7 Fig). The variations in the delta values in the profiles were also narrow, and there was no vertical trend (Figs 3.3n and o). The same trend was observed at K3, K10, K11, K12, V4, and A2, which were in the wet and intermediate areas (Table 2.1).

3.3.3. Isotopic composition of ground ice and water

Fig 3.4 shows the δD–$\delta^{18}O$ plot of river water from the Indigirka mainstream and tributaries, water in the thaw layer, ice in the frozen layer, precipitation, and snow cover obtained during the sampling periods. Precipitation data for summers in 2013 and 2014 and snow data obtained in 2014 and 2015 April are also shown. The δD and $\delta^{18}O$ values of the Indigirka mainstream water ranged from −177‰ to −155‰ and from −22.9‰ to −20.3‰, respectively. The δD and $\delta^{18}O$ values of the Indigirka tributaries water ranged from −171‰ to −140‰ and from −21.8‰ to −18.3‰, respectively, which are generally higher than the mainstream values. All of the river data slightly deviated below the Global Meteoric Water Line (GMWL) with d-excess of 0‰–8‰, which seems to be the mixing of summer precipitation with low d-excess and evaporated surface water.

The δD and $\delta^{18}O$ values of the soil water in the thaw layer in 2011 were from −177‰ to −115‰ and from −24.1‰ to −15.3‰, respectively, and those in 2012 were from −168‰ to −138‰ and from −22.3‰ to −18.2‰, respectively (S1 Table). The data in 2011 except for some samples with low delta values (δD and $\delta^{18}O$ were −177‰ and −24.1‰, respectively) and several high delta values (δD and $\delta^{18}O$ were from −121‰ to

−116‰ and from −16.2‰ to −15.3‰, respectively) were in a comparable range with the data in 2012, which were similar to the delta values in the Indigirka tributaries (Figs 3.4a and b). The δD and $\delta^{18}O$ values of ice in the frozen layer were lower than those of the water samples from the river and thaw layers with ranges from −193‰ to −144‰ and from −25.4‰ to −19.5‰, respectively. Most of the data of the thaw and frozen layers were plotted on or slightly below the GMWL.

The precipitation mostly had higher average δD and $\delta^{18}O$ values with the standard deviation (SD) during the summer sampling periods (June–August) in 2012 (−110±12‰ and −14.1±1.9‰, respectively), 2013 (−128±19‰ and −16.0±3.0‰, respectively) and 2014 (−129±28‰ and −16.8±3.7‰, respectively) than those of other samples from the river and water and ice in the soil. The soil water in the thaw layer had very high delta values (Fig 3.4a) close to the summer precipitation (Fig 3.4b).

The average δD, $\delta^{18}O$, and d-excess values with SD of the snow cover observed in 2014 (−226±13‰, −29.9±1.9‰ and 13±3‰, respectively) and 2015 (−205±19‰, −27.0±2.4‰ and 11±6‰, respectively) clearly had the lowest delta values.

3.4. Discussion

3.4.1. Relationship between the ground ice and the vegetation and microtopography

As described in the Results section, the tree mounds showed higher GWC in the frozen layer, shallower thaw depth, and higher relative elevation than the wet areas (Table 3.1). Ice-rich layers were only observed in the frozen layer of the tree mounds. Such data suggest that the presence of ground ice contributes to microtopographic features; namely, the higher elevation of the ground surface is due to frost heave (Van Everdingen, 1998).

On the other hand, the soil moisture in the thaw layer at tree mounds was smaller than that at wet areas (Liang et al., 2014; Morozumi et al., 2019). The vegetation of the higher elevation areas (tree mound) was larch trees and shrubs with green-moss and cowberry, whereas that of the lower elevation areas (wet area) was mainly sedges and sphagnum-moss. This vegetation structure and composition may depend on the differences in the microtopographic elevation and thaw depth (i.e., frost table elevation), which control the soil moisture condition (Boudreau and Rouse, 1995; Engstrom et al., 2005; Godin et al., 2016).

Similar results on the vegetation structure and composition corresponding to the microtopography have also been reported for Arctic tundra (Minke et al., 2009; Wolter et al., 2016; Zibulski et al., 2016). The surface elevation is also affected by the accumulation of mosses and organic matter from the vegetation. The vegetation and microtopography, which are affected by the ground ice, may interact with each other and form or change landscapes in this region.

There seem to be two prominent types and formation processes of ground ice in tree mounds. One is ice segregation as soil freezes. Massive ice segregation is likely to occur particularly at the transition zone, which is situated at the uppermost layer of permafrost and alternates in status between an active layer and permafrost over periods of less than a decade to multiple centuries (Shur et al., 2005; French and Shur, 2010). At K7 categorized into pattern (ii), the depth of approximately 60–90 cm showed high ice content, which was situated at the upper part of the frozen layer (Fig 3.3e and S7 Fig). This ice-rich layer led to the transition zone where ice segregation occurred. As described previously, pattern (ii) was observed in tree mounds. A higher surface elevation due to frost heave and the accumulation of organic matter or natural levees of former river channels (Morozumi et al., 2019; Sidorchuk et al., 2000) caused the low soil moisture condition. The lower thermal conductivity with the low soil moisture may have induced further ice segregation with slow freezing, as explained in the next section.

The second process is ice wedge formation due to the infiltration of snowmelt water in thermal contraction cracks (e.g., Mackey, 1983), which produces polygon mires (Chernov and Matveyeva; 1997). A high ice content of almost pure ice with a thickness of less than 10 cm was observed in the uppermost part (20–30 cm depth) of the frozen layer at K4 (Fig 3.3i and S7 Fig), which was categorized as pattern (iii). The ice wedges of pattern (iii), which were confirmed by isotopic composition as described in the next section, were also observed in tree mounds. The low soil moisture of tree mounds might help form thermal contraction cracks (Van Everdingen, 1998).

An ice-rich layer was not observed in the wet areas, which may have caused the lower elevation compared to tree mounds. Although the observed ice content in the frozen layer was small at the wet areas, the soil moisture was higher than the tree mounds (Liang et al., 2014; Morozumi et al., 2019). The thermal conductivity of the surface soil layer in the wet area could be high because of the greater soil moisture (Matsumoto and Ohkubo, 1977; Hinzman et al., 1991), which may lead to permafrost thawing in summer and quickly freezing in winter. For the tree mounds, the surface shrubs currently increasing in the Arctic region (Frost and Epstein, 2014; Kravtsova and Loshkareva, 2013), may inversely disturb permafrost thawing through the shading effect (Blok et al., 2010). The low soil moisture content (Liang et al., 2014; Morozumi et al., 2019), green-moss, and organic matter on the surface of the tree mounds are also important factors which decreased thermal conductivity (Matsumoto and Ohkubo, 1977; Hinzman et al., 1991). Lower thermal conductivity at the tree mounds may reduce permafrost thawing during summer and cause slow freezing in winter. As described above, our data suggest that the vegetation and microtopography also affect the ground ice.

3.4.2. Formation processes and isotopic compositions of the ground ice

The freezing rate, which depends on the thermal conductivity, is an important factor for ground ice formation in soil. It has been also reported that the minimum ground temperature during a winter at the top of permafrost also affected the formation of ground ice (e.g., Kokelj and Burn, 2005; Cheng, 1983). Kokelj and Burn (2005) showed a large difference in the minimum ground temperature at the top of permafrost among sites (more than 10 °C) at Mackenzie Delta, and this affected the difference in formation of ground ice. In our sites, however, minimum ground temperature was about −14 °C in the 2011 and 2012 winter, which was the same between tree mounds and wet areas (S5 and S6 Figs). Therefore, it is considered that there was no difference in the effect of the minimum ground temperature between tree mounds and wet areas for the formation of ground ice in the sites.

The freezing rate also affects isotope fractionation during freezing of water. The ice formation processes of each profile pattern were assessed according to the isotopic composition of the ground ice.

In the frozen cores categorized into pattern (ii), large variations in the delta values were observed for the ice-rich layer with high ice content (Figs 3.3e–g); this indicates isotope fractionation during ice formation. Prominent fractionation was observed at the depth of 60–90 cm in the frozen cores. These layers had high ice content, and the $\delta^{18}O$ values were also higher at the upper and lower parts of the layers (−21.8‰ and −22.9‰) than at the middle parts of the layers (from −25.7‰ to −24.7‰). The slope of the regression line of pattern (ii) in the δD–$\delta^{18}O$ plot was 6.9 (Fig 3.4c), which suggested a near equilibrium isotope fractionation during freezing (Suzuoki and Kjmura, 1973; Lacelle, 2011; O'Neil, 1968). The $\delta^{18}O$ value of ice has been reported to be enriched by 2.8–3.1‰ compared to the source water when frozen under equilibrium conditions (Suzuoki and Kjmura, 1973; O'Neil, 1968). If the initial $\delta^{18}O$ value of the water was −23.8‰, which was the average $\delta^{18}O$ at a depth of 60–90 cm, the $\delta^{18}O$ value of the first ice will be from −21.0‰ to −20.6‰. That of the subsequent ice will gradually decrease and finally be quite lower than the initial value. Therefore, it is indicated that the upper part (60 cm depth) and the lower part (90cm depth) were formed at first (higher $\delta^{18}O$ values), and then the ice of middle part at the depth of 60–90 cm was formed (lower $\delta^{18}O$ values). Observed $\delta^{18}O$ values of the first ices were slightly lower than the theoretical values due to thickness of the sampling.

The equilibrium fractionation during freezing occurs when the freezing rate is less than the HDO and $H_2{}^{18}O$ diffusion rates (Lacelle, 2011). The slow freezing may provide sufficient time for unfrozen soil water to slowly migrate to the freezing front (S1 Appendix). Soil freezing in winter generally starts from the upper side because of the cooling air temperature, and also from the lower side because of the permafrost. Therefore, the unfrozen soil water apparently migrated to both freezing fronts and formed thick ice lenses (S2 Appendix), so higher ice contents were observed at the depths of 60 and 90 cm (917% and 542%, respectively), and lower ice content was observed at the middle part between them (149%) (Fig 3.3e).

The delta values tended to decrease from the surface soil to the deeper frozen layer in most of the samples categorized in pattern (i), as shown in Figs 3.3b and c. These trends suggest Rayleigh-type fractionation of the stable water isotopes during freezing (e.g., Lacelle, 2011; Souchez and Jouzel, 1984; Fritz et al., 2011; Lacelle et al., 2014). Additionally, discontinuities in the profiles of the delta values and d-excess were observed at a depth of 52–61 cm (Figs 3.3b–d), which indicates thaw unconformity. This depth appears to be the maximum depth of the active layer (S5 and S6 Figs). The decrease in the delta values may have been caused by isotopic fractionation during freezing and developed above and below the layers of the thaw unconformity separately.

Pattern (iii) showed a high ice content at the uppermost frozen layer (551% in Fig

3.3i) with $\delta^{18}O$ and δD values of −22.0‰ and −166‰, respectively. On the other hand, the delta values of the lowermost thaw layer were low ($\delta^{18}O$ of −24.1‰ and δD of −177‰), and the d-excess value was high at 15‰ (Figs 3.3j–l). This suggests a large contribution from snowmelt water. As indicated in Fig 3.4b and S1 Table, snow cover showed low δD and $\delta^{18}O$ values with high d-excess. The δD and $\delta^{18}O$ values (and d-excess) observed in 2014 were −226±13‰ and −29.9±1.9‰ (and 13±3‰), respectively, and those in 2015 were −205±19‰ and −27.0±2.4‰ (and 11±6‰), respectively. The snowmelt water mixed with soil moisture from the previous summer may have been source water of the ice. This water infiltrated from the surface to the frozen layer and then froze as an ice wedge because the air temperature was greater than 0 °C and the frozen ground was colder than 0 °C.

The difference between the isotopic values of the lowermost thaw layer and ice wedge (approximately 2‰ for $\delta^{18}O$ and 4‰ for d-excess) in pattern (iii) may have been due to isotope fractionation. We sampled the ice wedge separately from just below the frozen layer as seen in S7 Fig. Therefore, we obtained the $\delta^{18}O$ of total ice of the ice wedge, and compared with soil moisture in the thaw layer. This difference was slightly lower than the theoretical values (2.8‰ for $\delta^{18}O$) if we used the fractionation factor by Suzuoki and Kimura (1973). This observational result showed that fractionation factor was slightly lower, and freezing rate was slightly larger than the diffusion rates, leading to the fluctuation of the delta values decreased (Suzuoki and Kjmura, 1973; Lacelle, 2011). Although the freezing rate does not affect the ice wedge formation directly, the location where the ice wedge formed was at the sites with slow freezing rates, such as tree mounds with low soil moisture (and thus low thermal conductivity). This environment may be an important factor to suppress the thawing and growth of ice wedges.

The frozen layer in pattern (iv) had alternating layers of fine ice lenses and clays with low ice content of approximately 130% (Fig 3.3m and S7 Fig). In other words, there was no ice-rich layer. The d-excess value seemed to be lower for the frozen layers of the wet areas than for the tree mounds (Table 3.1), and the slope of the regression line between δD and $\delta^{18}O$ of pattern (iv) was 4.5 (Fig 3.4c), which is considerably less than that of the other patterns. Such data suggest that the ice freezing occurred rapidly (i.e., under relatively non-equilibrium conditions) in the layer (Suzuoki and Kjmura, 1973; Lacelle, 2011). This rapid freezing, especially when the freezing rate was far greater than the HDO and $H_2^{18}O$ diffusion rate, does not allow sufficient time for ice segregation (S1 Appendix) and isotopic fractionation to occur. Accordingly, the ice content stayed low (i.e., an ice-rich layer did not form), and the delta values were almost constant for pattern (iv). The rapid freezing may have been due to the relatively high thermal conductivity.

The different thermal conductivity in the surface soil coexisting in the same area (i.e., the different freezing rates between tree mounds and wet areas) may depend on the vegetation and microtopography. The main controlling factors of the thermal conductivity are the soil moisture (Matsumoto and Ohkubo, 1977; Hinzman et al., 1991), snow cover (Zhang, 2005), and organic soil (Hinzman et al., 1991). Compared to the wet areas, the tree mounds had lower soil moisture (Liang et al., 2014; Shingubara et al., 2019; Morozumi et al., 2019), and thicker snow cover (e.g., Essery and Pomeroy, 2004; Hirashima et al., 2004). There was no difference in the depth of organic layer (Table 3.1), although more leaves fell down from the trees. Therefore, the thermal conductivity in winter (i.e., the freezing rate) of the tree mounds was likely lower than that of the wet areas.

There was no difference in average water isotope values of frozen layers between tree mounds and wet areas (Table 3.1), and these isotope values (δD-$\delta^{18}O$) were plotted between summer precipitation and snow cover (Fig 3.4). Therefore, it is clear that the mixture of summer precipitation and snow cover infiltrated the soil, and served as a source of the ground ice. However, it is unclear when this water was infiltrated and formed ices, because currently the tree mounds with dryer surface soils show more ground ice in frozen layers than in wet areas. One possibility might be that unfrozen water in the frozen ground where rapid freezing occurred (i.e., wet areas) had migrated to the freezing front which slowly freezing occurred (i.e., tree mounds).

During *in situ* freezing of soil, the freezing rate might be affected by such as the presence of unfrozen water in the soil, differences in soil particles, and heterogeneous soil temperature. They are further complicated by the combination of these factors, and the freezing is not clearly differentiated between the equilibrium or non-equilibrium conditions. There are many unknown points about the *in situ* freezing of soil, which requires further investigation.

The freezing rate (i.e., the thermal conductivity in the surface soil) affects the formation of the ground ice, therefore, the future changes in the snow cover, soil moisture, and organic layer predicted in models (e.g., Raisanen, 2008; Ise et al., 2008; Allison et al., 2010; Callaghan et al., 2011; Bring et al., 2016) can impact the freezing environment of the ground ice. In addition, a warming trend has been reported for the permafrost in northeastern Siberia (Romanovsky et al., 2007; 2010), and numerical models have calculated significant degradation of the permafrost during the 21st century (Koven et al., 2011; Lawrence et al., 2012). This suggests that a difference in the relative elevation (i.e., microtopography) may be reduced by a loss of ground ice thickness, which can have a significant impact on the vegetation structure and composition in northeastern Siberia. To reduce the uncertainty over the future conditions of the ground ice, the response of the soil environment (i.e., soil moisture, organic soil) to climate change needs to be further investigated.

3.5. Summary

In the current study, we investigated the spatial distribution of the ice content and the stable isotopic composition of ice and water in the near-surface permafrost to a depth of 1 m in relation to the vegetation and microtopography of the Taiga–Tundra boundary in the Indigirka River lowlands of northeastern Siberia. An ice-rich layer was observed in the tree mounds (microtopographically high elevation areas with growing larch trees), which had a significantly higher GWC than in the wet areas (lower elevation with wetland vegetation). This suggests that the relatively high microtopography of the land surface due to frost heave strongly affects vegetation composition. The water isotopic composition of the ground ice indicated that ice segregation occurred under close to equilibrium condition (slow freezing) in the tree mounds, whereas the near-surface ground in the wet areas froze under relatively non-equilibrium conditions (rapid freezing). Our results suggest that the lower thermal conductivity in the surface soil (i.e., the slower freezing rate) of the tree mounds compared with the wet areas was due to lower soil moisture and thicker snow cover.

Table 3.1. Summary of geological and isotopic parameters at the tree mounds and wet areas.

	All sites			Site K		
	tree mound	wet area	significance	tree mound	wet area	significance
Thaw depth (cm)	19.9 ±3.3	30.3 ±6.7	***	18.8 ±2.9	28.6 ±5.0	**
Depth of organic layer (cm)	31.6 ±24.0	26.9 ±8.6	none	36.4 ±27.2	30.8 ±9.6	none
Gravimetric water content of frozen layer (%)	167.3 ±71.1	92.6 ±20.0	***	206.3 ±58.9	100.6 ±19.5	***
$\delta^{18}O$ of frozen layer (‰)	-21.9 ±0.8	-21.6 ±0.3	none	-21.9 ±1.0	-21.5 ±0.2	none
$\delta^{18}O$ of thaw layer (‰)	-20.3 ±1.6	-19.9 ±1.4	none	-20.9 ±1.2	-20.9 ±0.9	none
$\Delta\delta^{18}O$ of frozen layer (‰)	2.9 ±0.9	2.0 ±1.1	**	2.7 ±0.7	1.5 ±0.3	***
d-excess of frozen layer (‰)	8.1 ±1.9	5.4 ±3.4	*	7.2 ±1.8	3.6 ±2.5	**
d-excess of thaw layer (‰)	10.0 ±2.3	9.1 ±1.3	none	9.3 ±2.4	9.2 ±1.3	none
Relative elevation (cm)				46.4 ±11.3	21.0 ±16.9	**

The average values with the standard deviation (SD) were obtained for all sites and at site K separately. The statistical significance of the differences between the tree mounds and wet areas were as follows: * = $p < 0.1$, ** = $p < 0.05$, *** = $p < 0.01$, and none = no difference at the 90% significant level.

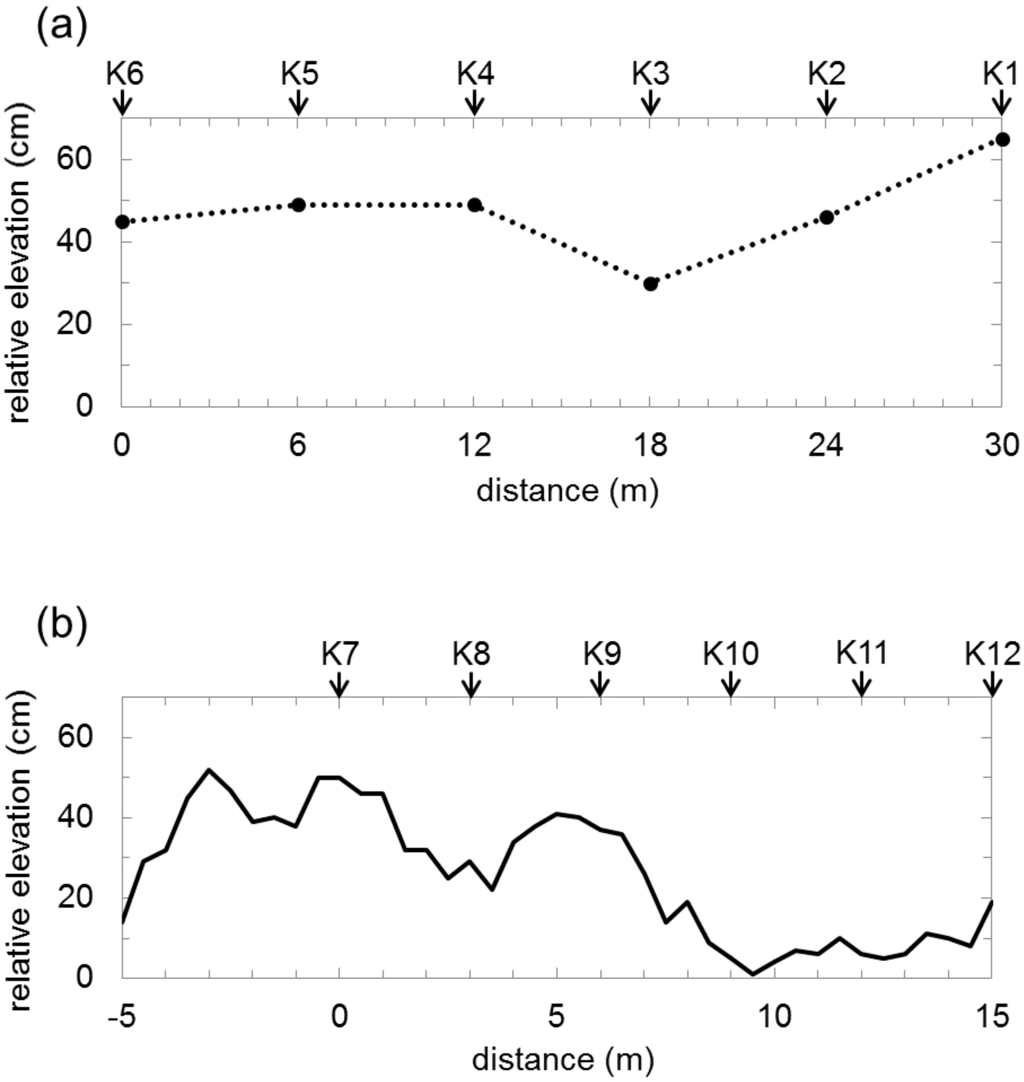

Fig 3.1. Relative elevations of the transect sampling points in Fig 2. (a) K1–K6 and (b) K7–K12. The relative elevations were determined based on the lowest point (0 cm) in the transects. Because the relative elevations were measured only at the boreholes in (a), the dotted line does not show the microtopography between boreholes.

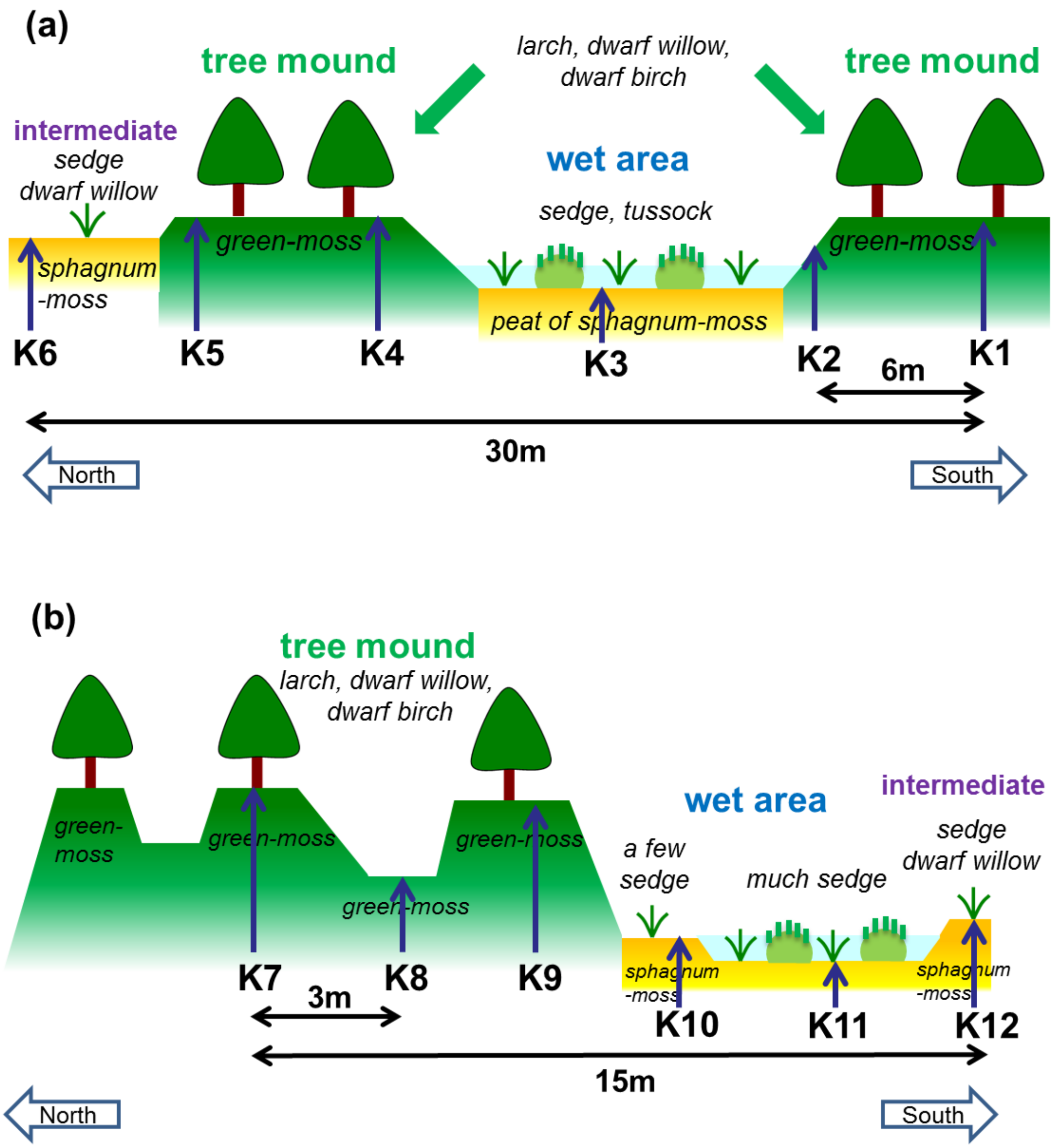

Fig 3.2. Vegetation and microtopography at the transect sampling points. (a) K1–K6 and (b) K7–K12.

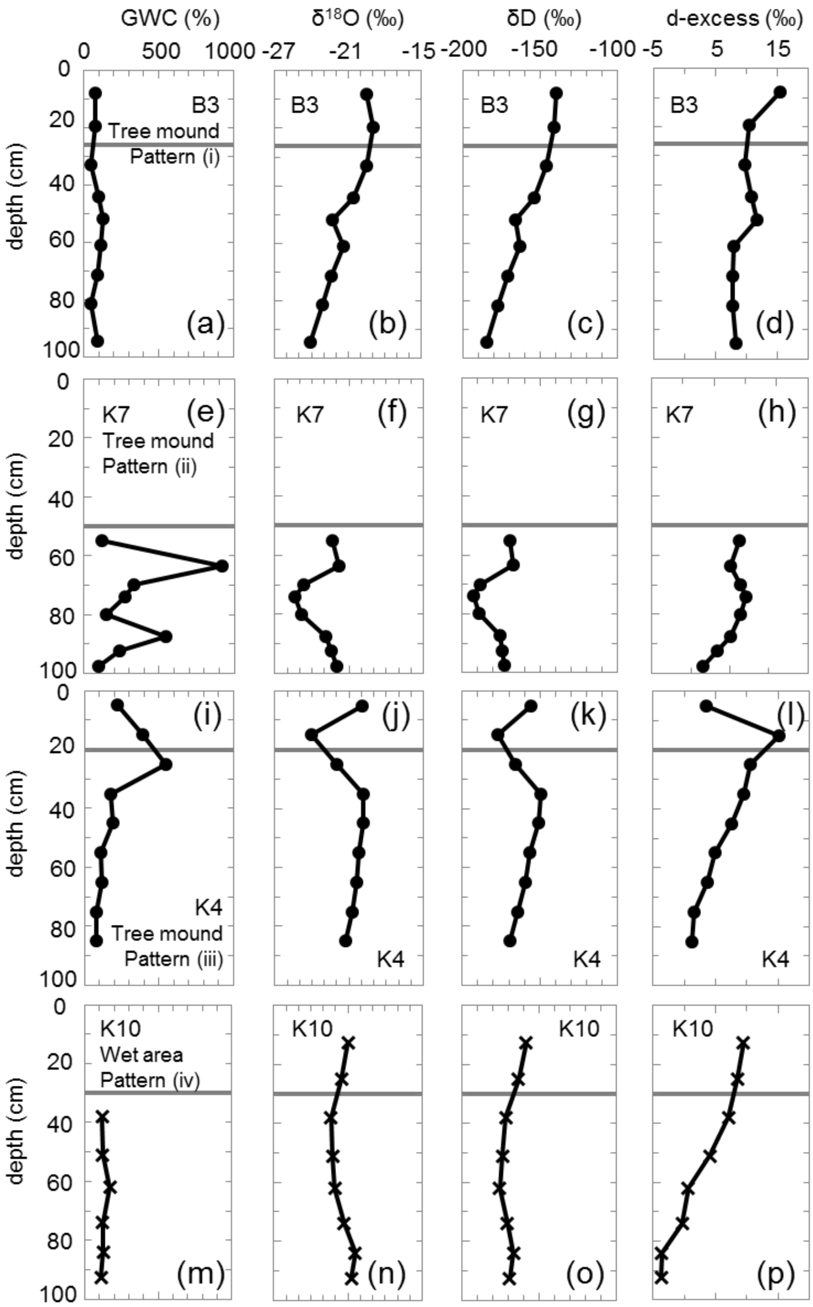

Fig 3.3. Vertical profiles of the gravimetric water content (GWC) and isotopic compositions of boreholes. (a) GWC, (b) $\delta^{18}O$, (c) δD, and (d) d-excess values of borehole B3. (e)–(p) data for K7, K4, and K10. The horizontal line in each figure represents the frozen table, and the vegetation and microtopography (tree mounds or wet areas) and patterns (i–iv) described in the Results section are also shown.

(a)

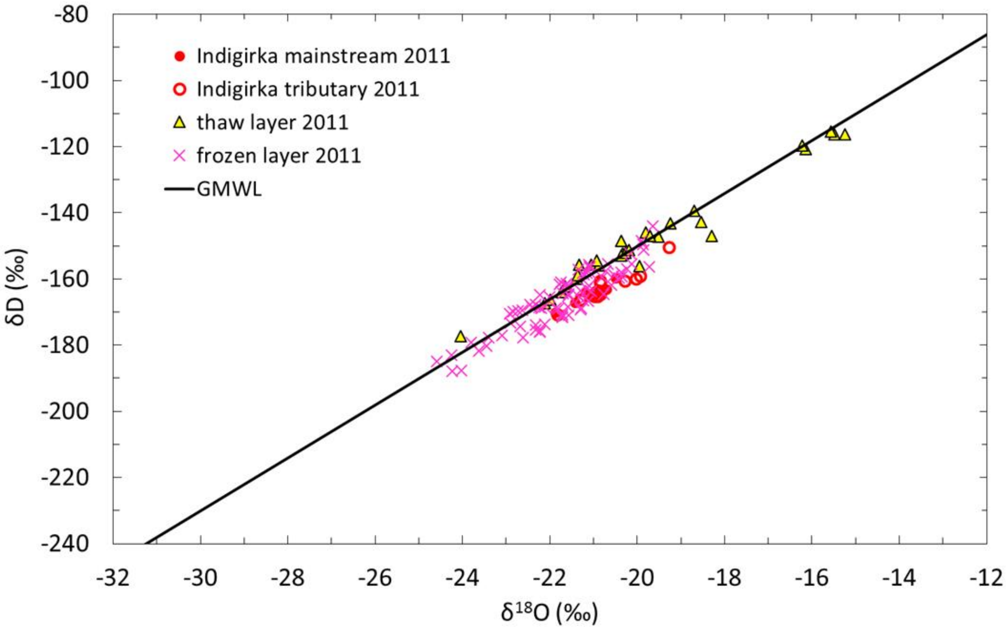

Indigirka mainstream 2011
Indigirka tributary 2011
thaw layer 2011
frozen layer 2011
GMWL
δD (‰)
δ18O (‰)

(b)

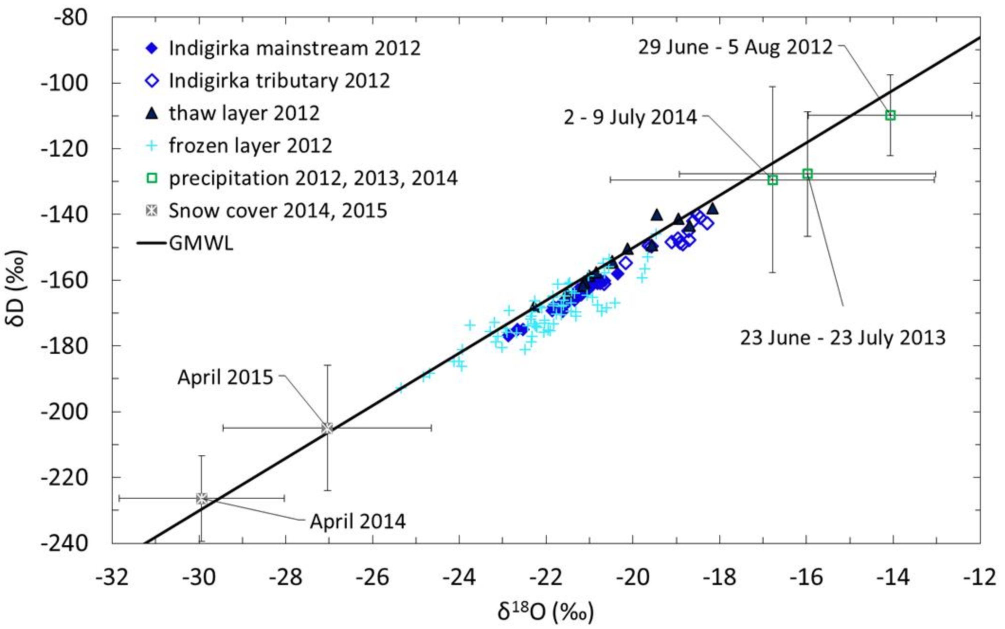

Indigirka mainstream 2012
Indigirka tributary 2012
thaw layer 2012
frozen layer 2012
precipitation 2012, 2013, 2014
Snow cover 2014, 2015
GMWL
29 June - 5 Aug 2012
2 - 9 July 2014
23 June - 23 July 2013
April 2015
April 2014
δD (‰)
δ18O (‰)

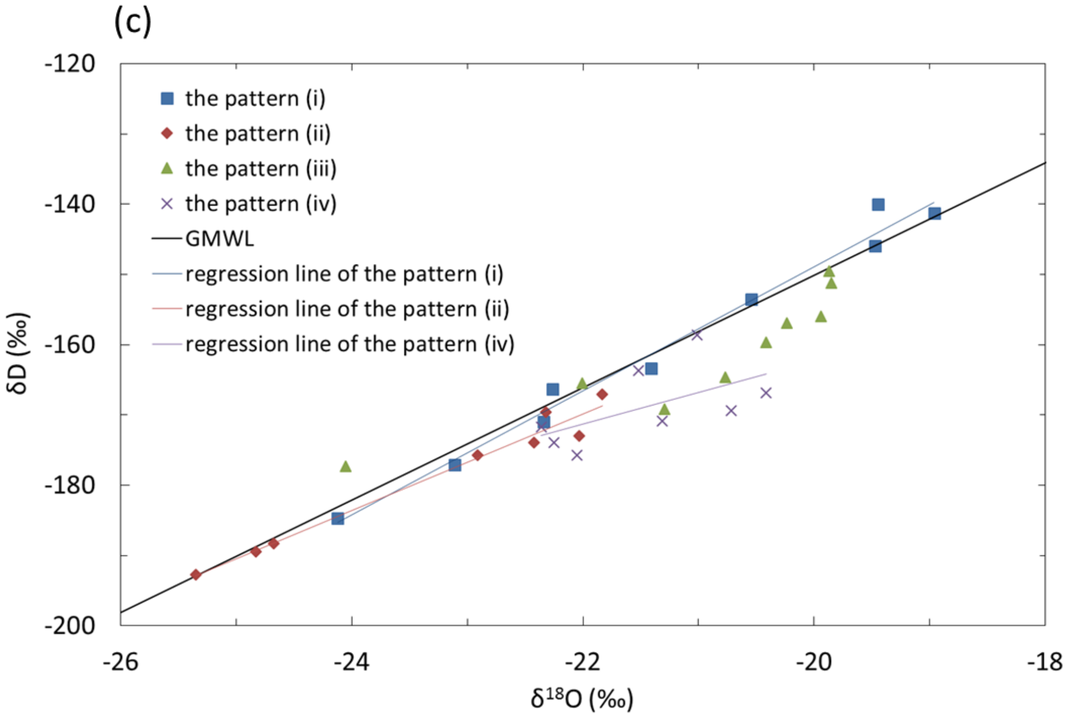

Fig 3.4. δD–δ^{18}O plot for water, ice, and snow samples with the Global Meteoric Water Line (GMWL; δD = 8 × δ^{18}O + 10). (a) The δD–δ^{18}O plot was obtained for water from the Indigirka mainstream and tributaries, water and ice in the thaw and frozen layers during the summer sampling period in 2011 and (b) similar data observed in 2012. The isotopic compositions of precipitation were observed in 2012, 2013, and 2014. The snow cover was obtained in April 2014 and April 2015. The isotopic compositions of the precipitation and snow cover are shown with the SD. (c) The δD–δ^{18}O data of B3, K7, K4, and K10 are plotted as profile patterns (i), (ii), (iii), and (iv). The regression equations of patterns (i), (ii), and (iv) are δD = 8.8 × δ^{18}O + 27, δD = 6.9 × δ^{18}O – 19, and δD = 4.5 × δ^{18}O − 73, respectively.

S1 Table. Summary of the δD, $\delta^{18}O$, and d-excess results for the water, ice and snow samples. The maximum, minimum, and average values with the SD and the number (n) of samples observed for each year are presented.

	Year	δD (‰)			$\delta^{18}O$ (‰)			d-excess (‰)			n
		Max	Min	Average ± SD	Max	Min	Average ± SD	Max	Min	Average ± SD	
Indigirka mainstream	2011	-160	-170	-164 ± 3	-20.5	-21.9	-21.0 ± 0.4	5	2	4 ± 1	11
	2012	-158	-177	-165 ± 5	-20.3	-22.9	-21.3 ± 0.6	8	3	6 ± 1	29
Indigirka tributary	2011	-150	-171	-163 ± 5	-19.3	-21.8	-20.7 ± 0.6	6	0	3 ± 2	15
	2012	-140	-161	-148 ± 6	-18.3	-20.7	-19.1 ± 0.7	8	2	5 ± 2	14
thaw layer	2011	-115	-177	-148 ± 16	-15.3	-24.1	-19.7 ± 2.2	15	-1	10 ± 3	29
	2012	-138	-168	-153 ± 9	-18.2	-22.3	-20.3 ± 1.2	16	6	9 ± 2	14
frozen layer	2011	-144	-188	-166 ± 9	-19.7	-24.6	-21.7 ± 1.1	14	1	8 ± 4	79
	2012	-146	-193	-170 ± 9	-19.5	-25.4	-22.0 ± 1.2	16	-4	6 ± 4	71
precipitation	2012	-82	-127	-110 ± 12	-10.2	-17.0	-14.1 ± 1.9	10	-3	3 ± 5	12
	2013	-104	-161	-128 ± 19	-12.4	-21.0	-16.0 ± 2.9	8	-17	0 ± 9	9
	2014	-105	-187	-129 ± 28	-13.5	-24.3	-16.8 ± 3.7	8	1	5 ± 2	7
snow cover	2014	-200	-275	-226 ± 13	-25.5	-36.5	-29.9 ± 1.9	20	4	13 ± 3	37
	2015	-172	-258	-205 ± 19	-22.8	-33.4	-27.0 ± 2.4	22	-5	11 ± 6	37

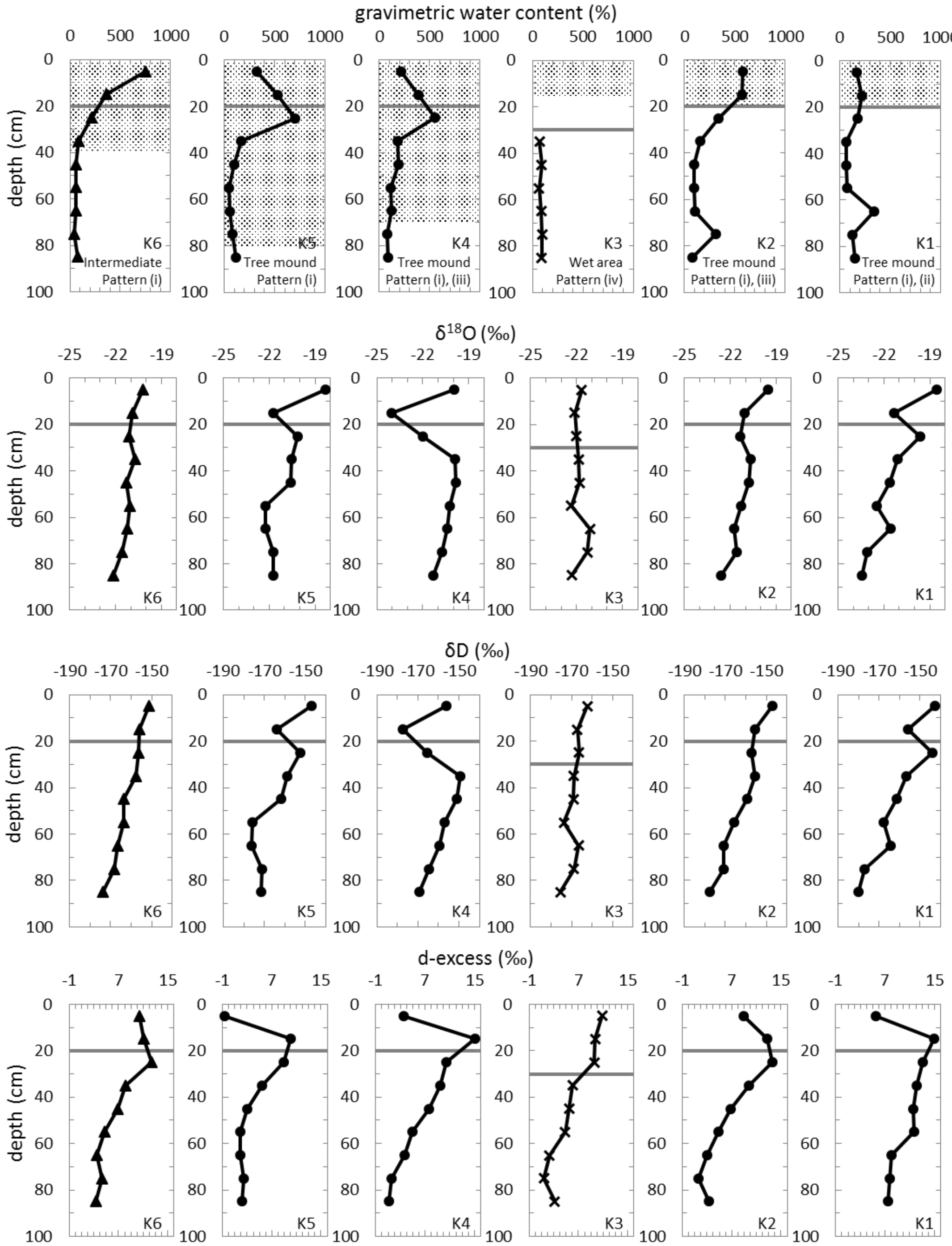

S1 Fig. Vertical profiles of the gravimetric water content (GWC) and isotopic compositions of boreholes obtained at site K in 2011. The upper panels show the GWC and the lower panels show $\delta^{18}O$, δD, and d-excess values for the observed data at K6, K5, K4, K3, K2, and K1. The horizontal line in each figure represents the frozen table.

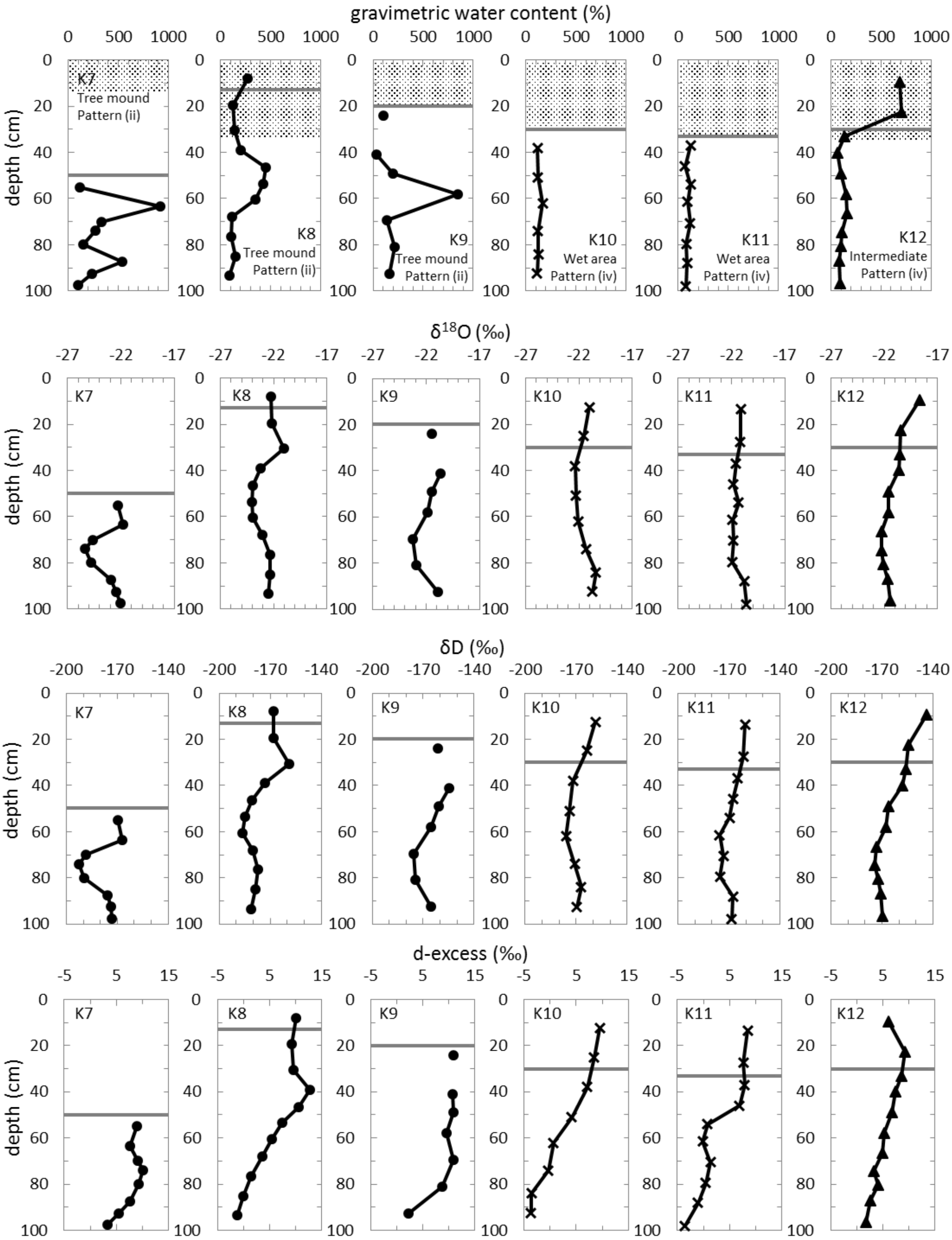

S2 Fig. Vertical profiles of the gravimetric water content (GWC) and isotopic compositions of boreholes obtained at site K in 2012. The data are similar to those in S1 Fig but for K7, K8, K9, K10, K11, and K12.

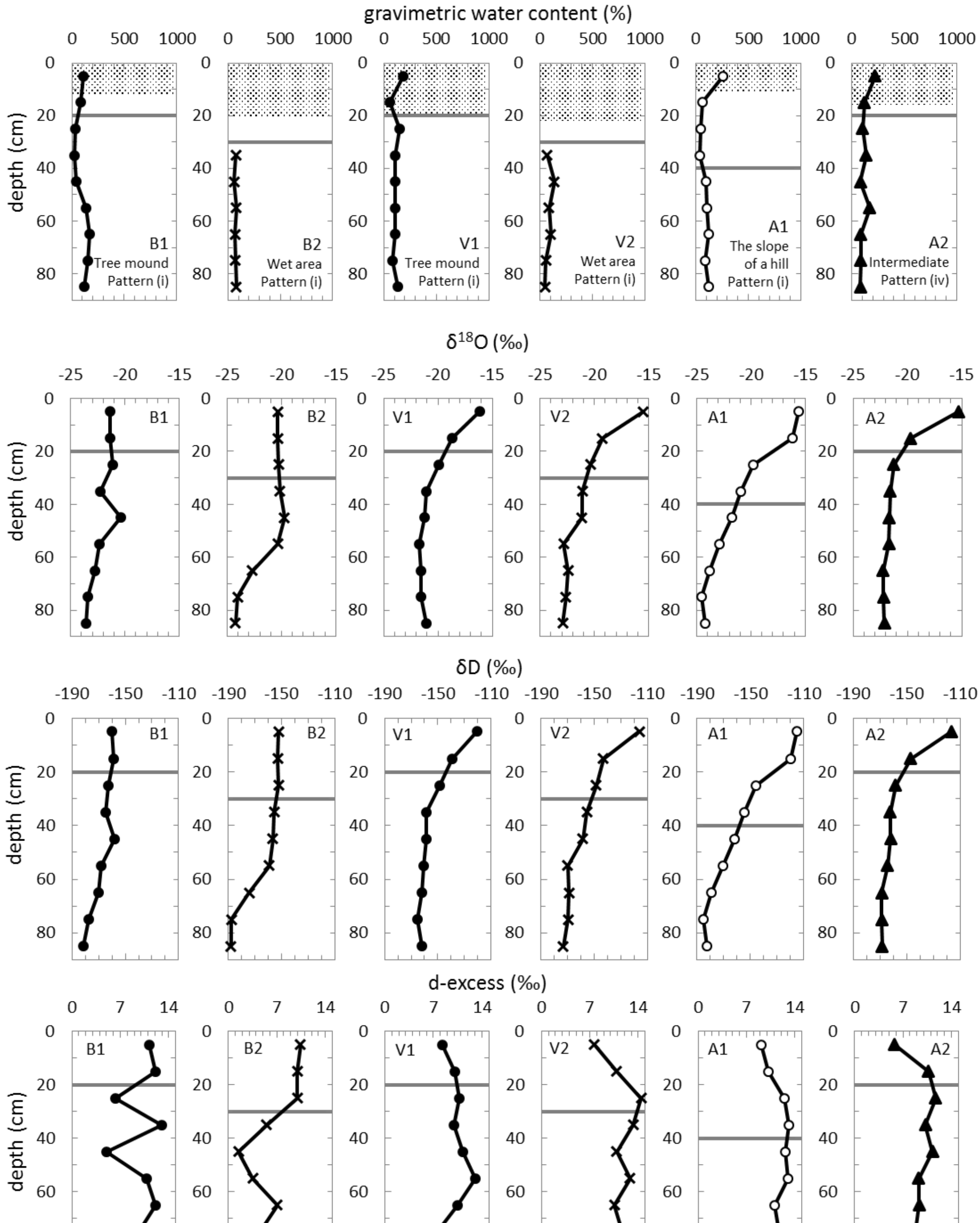

S3 Fig. Vertical profiles of the gravimetric water content (GWC) and isotopic compositions of boreholes obtained at sites B, V, and A in 2011. The data are similar to those in S1 Fig but for B1, B2, V1, V2, A1, and A2.

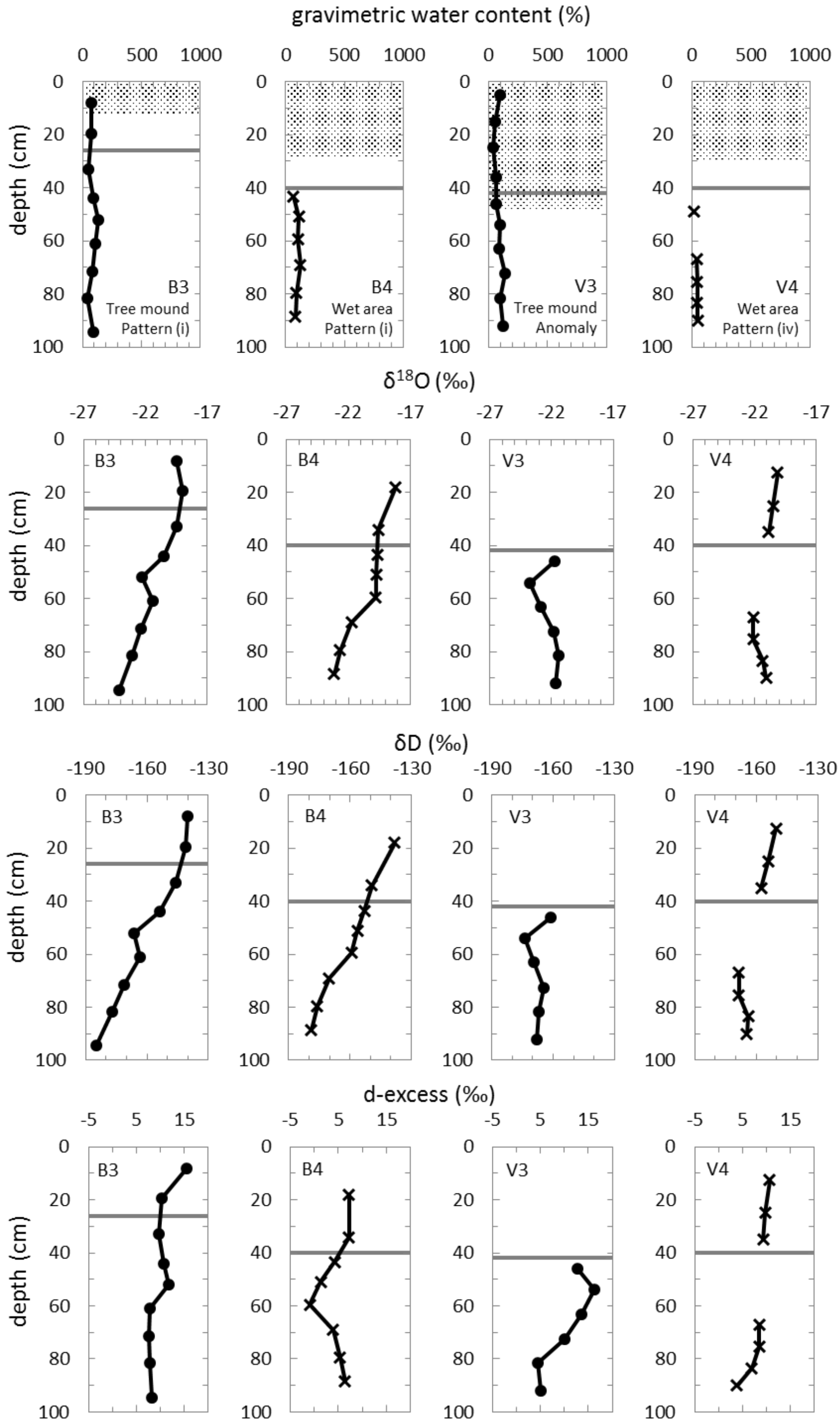

S4 Fig. Vertical profiles of the gravimetric water content (GWC) and isotopic compositions of boreholes obtained at sites B, V, and A in 2012. The data are similar to those in S1 Fig but for B3, B4, V3, and V4, respectively.

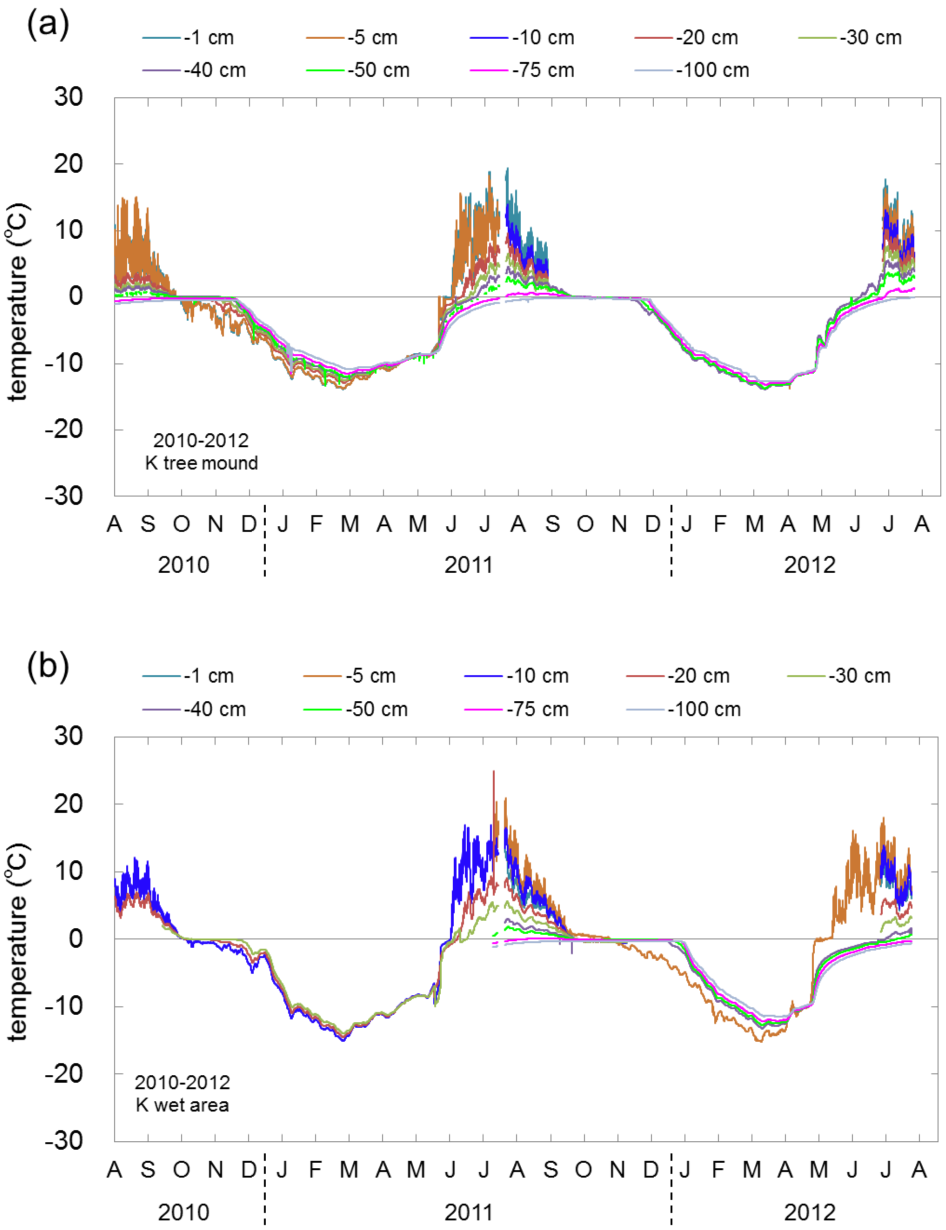

S5 Fig. Seasonal variation in ground temperature from August 2010 to July 2012 at site K. The seasonal variations in ground temperature from the surface to 100 cm depth at (a) tree mound and (b) wet area. The ground temperature was measured with thermistor sensors (TMC-HD; Onset Computer Co.) and recorded by data loggers (HOBO U12-006; Onset Computer Co.). Gaps in the time series or absence of the data shows missing data. The data from August 2010 to July 2011 were also reported by Iwahana et al. (2014).

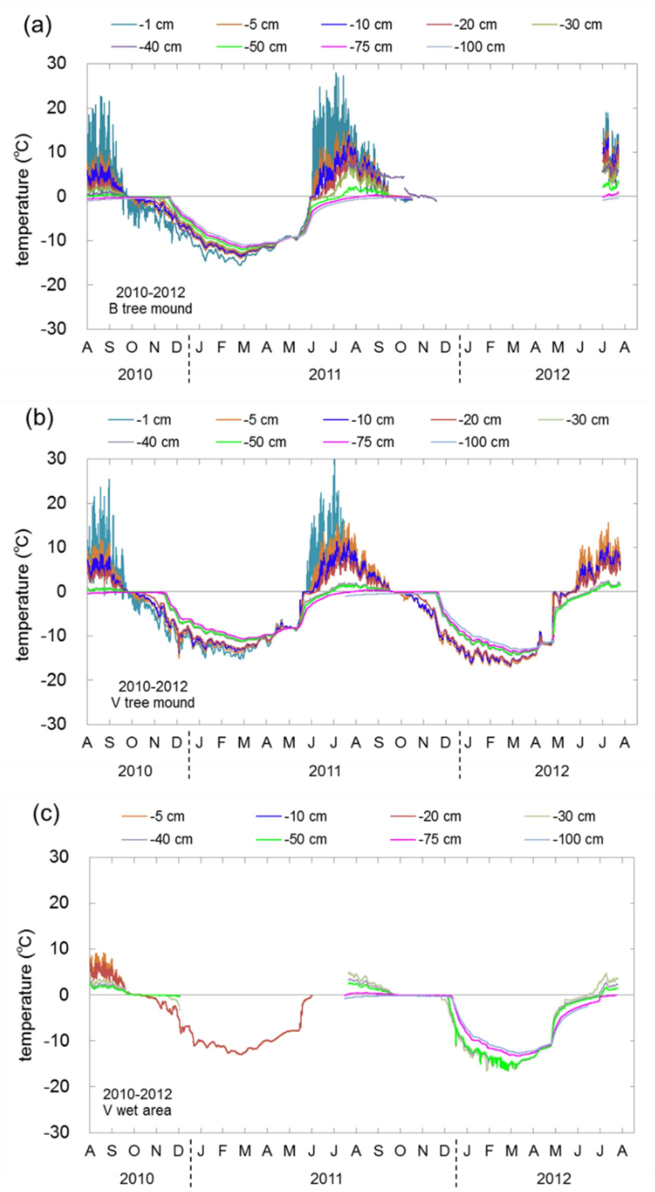

S6 Fig. Seasonal variation in ground temperature from August 2010 to July 2012 at sites B and V. The seasonal variations in ground temperature from the surface to 100 cm depth at (a) tree mound of site B, (b) tree mound of site V, and (c) wet area of site V. The ground temperature was measured with thermistor sensors (TMC-HD; Onset Computer Co.) and recorded by data loggers (HOBO U12-006; Onset Computer Co.). Gaps in the time series or absence of the data shows missing data. The data from August 2010 to July 2011 were also reported by Iwahana et al. (2014).

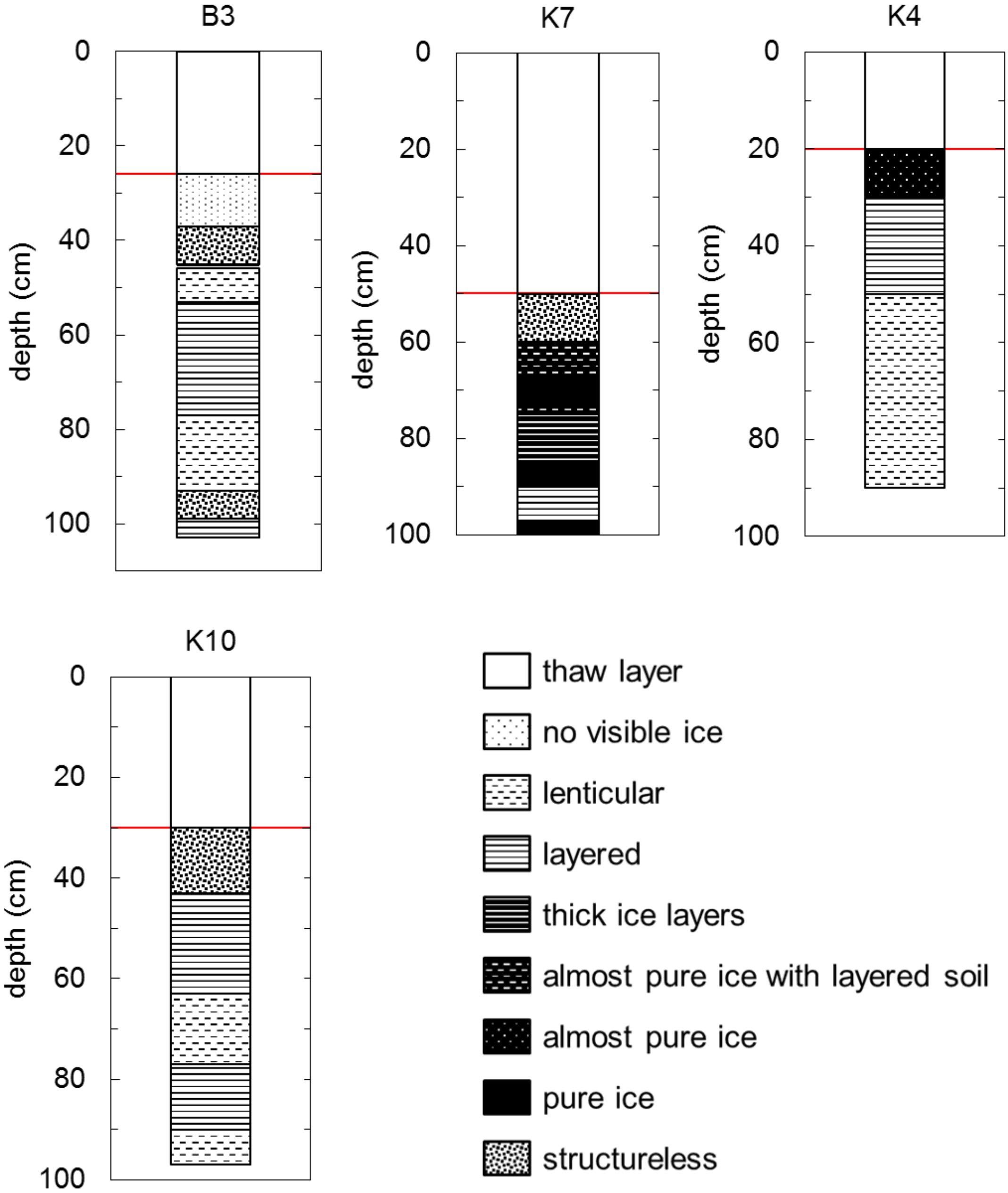

S7 Fig. Cryostructures of core samples B3, K7, K4, and K10. Examples of cryostratigraphic features in frozen layer of the study sites were reported in Iwahana et al. (2014).

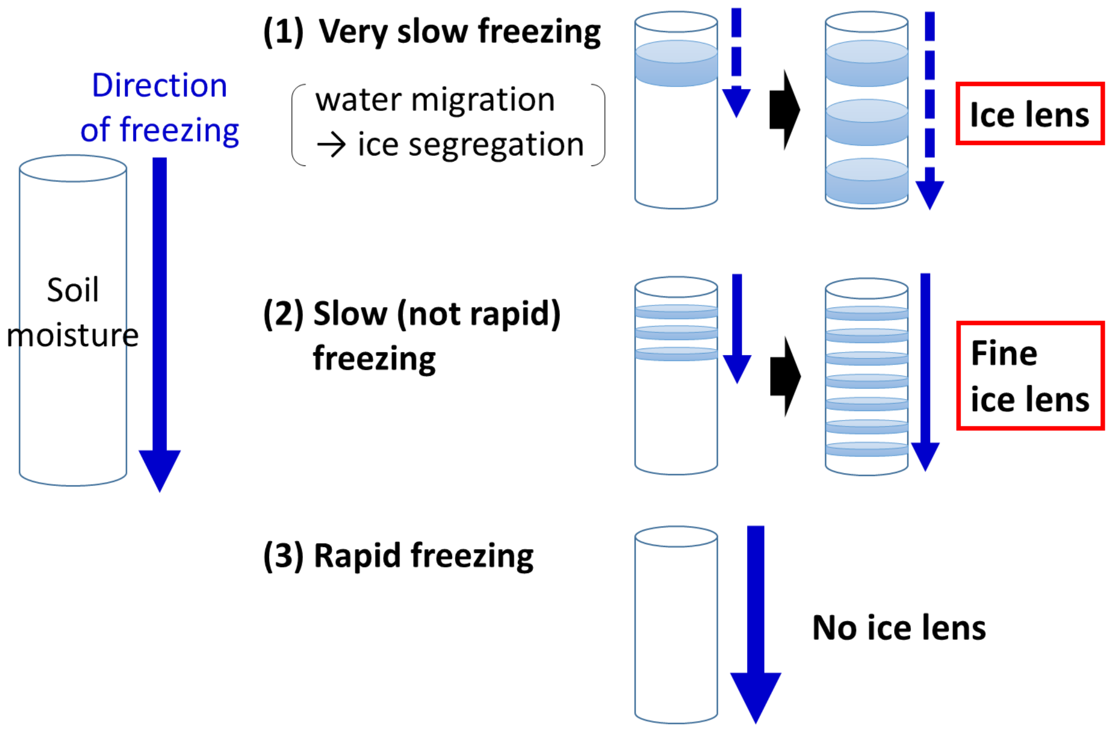

S1 Appendix. Freezing rate and ground ice forming. Slow freezing can provide sufficient time for unfrozen soil water to slowly migrate to the freezing front, resulting ice segregation, and form thick ice lenses (1). If the freezing rate is getting faster, the water migration (i.e., the ice segregation) is limited, then forming fine ice lenses (2). Further faster freezing (i.e., rapid freezing) does not allow sufficient time for ice segregation, resulting no ice lens in frozen soil (3).

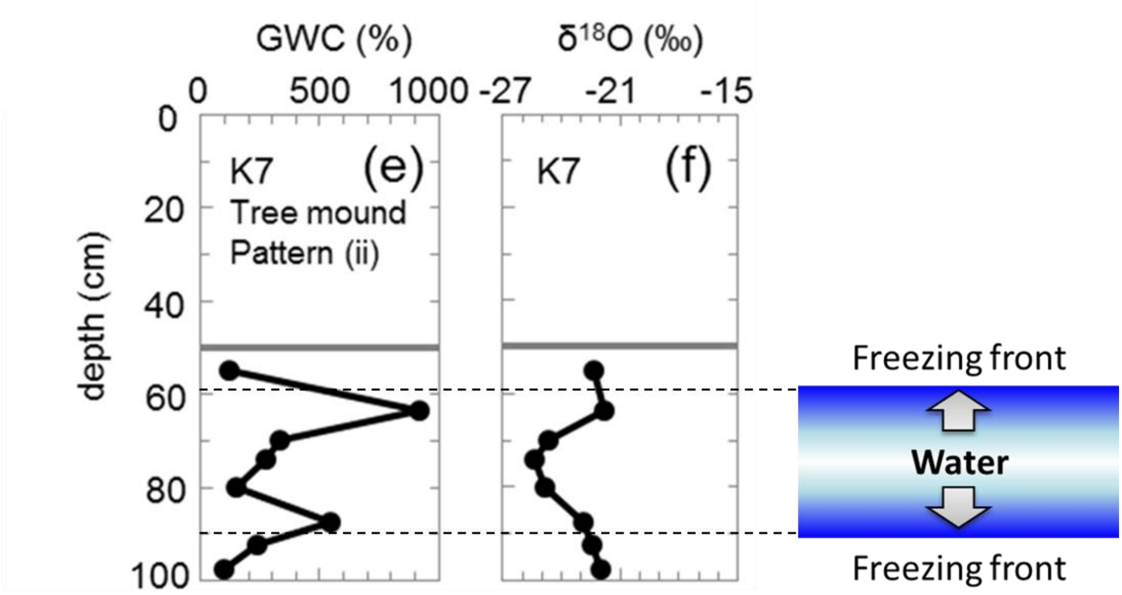

S2 Appendix. Vertical profiles of the gravimetric water content (GWC) and δ^{18}O of borehole obtained at K7 classified to the pattern (ii), and unfrozen soil water migration during freeze between the depths of 60 and 90 cm. The unfrozen water apparently migrated to the upper and lower freezing fronts, resulting first ices with higher ice contents and higher δ^{18}O and last ice (the middle part of the depth) with lower ice contents and lower δ^{18}O.

Chapter 4. Snow cover properties at Taiga-Tundra boundary in the Indigirka River lowlands, northeastern Siberia

4.1. Introduction

Snow cover in Arctic region is one of the important factors controlling surface water balance, energy fluxes, as well as ecosystem and permafrost dynamics (e.g., Stow et al., 2004; Ling and Zhang, 2007; Elberling, 2007, Larsen et al., 2007). However, the impact of changing winter season temperature and precipitation (e.g. Brown and Mote, 2009) on variables such as snow water equivalent (SWE) is less clear (Raisanen, 2007, 2008; Derksen et al., 2010; Callaghan et al., 2011; Bring et al., 2016).

Quantifying the spatial and temporal variations in snow depth, density and SWE is essential for many applications in hydrology and ecology, such as water budget and soil moisture, but generalizing regional snow distribution in Arctic region is not a simple task. Snow accumulation patterns at the regional scale in the tundra are controlled by not only difference in precipitation but also by the complex interaction of blowing snow (re-distribution) with vegetation and microtopography (e.g. Essery and Pomeroy, 2004; Hirashima et al., 2004; Rees et al., 2014), and sublimation (25-50% of total snowfall) (e.g. Pomeroy et al., 1997, 1998; Liston and Sturm, 1998; Essery et al., 1999; Pomeroy and Essery, 1999).

While point data are useful and often considered most accurate, the predominant need for Arctic snow cover data is to be scaled up to regional grids of several km^2. The purposes of this study are to know the spatial variations in snow depth, snow density, SWE and stable isotopic composition of snow in Indigirka River lowland near Chokurdakh, and to estimate average SWE for regional scale (approximately 100 km^2).

4.2. Methods

4.2.1. Sampling area

Detailed data were obtained on the vegetation, which as classified into several classes (including tree, shrub, willow, cotton-sedge, *Sphagnum*, emergent, bare-land, and lake/river) based on plant species identified by Morozumi et al. (2019). In this chapter, the tree, shrub, and willow classes were grouped into “larch/shrub”, the cotton-sedge, *Sphagnum*, emergent, and bare-land classes were grouped into “sedge/sphagnum”, and the lake/river class was labeled as “river/lake”.

4.2.2. Snow sampling and measurements

Snow survey was conducted in 23–26 April 2014 and 15–17 April 2015 near Chokurdakh (Figure 4.1). Approximately 40 km north–south transect was set across the study area, sampling points along the transect were 11 and 12 in 2014 and 2015, respectively (Figure 4.2). In Kodac site (site K; Figure 4.1b, c), in which the landscape consisted of typical Taiga–Tundra boundary ecosystem, east–west transect was set across different vegetation types and observed at 25 points and 24 points in 2014 and 2015, respectively (Figure 4.3). The snow survey team traveled to each sampling point by snowmobile, and these locations (latitude, longitude, and elevation) were recorded by handheld GPS (etrex, Garmin, USA).

At each sampling point, a manual snow prove was done. Snow depth was measured and snow cover was obtained as a core with a diameter of 10 cm and put into a plastic bag. Some samples were obtained with 10-cm vertical resolution. The weight of each snow core was scaled using a balance with precision of ±1 g. Snow density and snow water equivalent (SWE) were directly calculated using the snow depth and the weight of the snow core. These data were summarized in Table 4.1. The snowmelt water samples were taken for isotope analysis and stored in glass vials soon after the melting snow in the plastic bags.

4.2.3. Statistical analysis

Steel-Dwass test was used to examine differences in the parameters of snow cover on the different vegetation.

4.3. Results

4.3.1. Spatial distribution of snow cover

The spatial distribution in SWE along the 40 km north–south transect was from 82.8 mm to 187.3 mm in 2014 and from 20.5 mm to 162.0 mm in 2015 (Figure 4.4a, c and Table 4.1). Among them, the SWE on larch/shrub ranged from 97.5 mm to 187.3 mm and from 97.8 mm to 162.0mm in 2015.

At site K, the spatial distribution in SWE ranged from 61.5 mm to 216.9 mm and from 41.4 mm to 161.8 mm in 2015 (Figure 4.4b, d and Table 4.1).

4.3.2. Snow properties with different vegetation

Figure 4.5 showed the snow parameters (snow depth, snow density, SWE, and $\delta^{18}O$ of snow cover) observed at each sampling point, and the average values and SD for each parameter were summarized in Table 4.2 for each vegetation of larch/shrub, sedge/sphagnum, and river/lake. The snow depth on larch/shrub, sedge/sphagnum, and river/lake in 2014 were 68.7 ±9.6 cm, 45.9 ±7.5 cm, and 41.0 ±8.2 cm, respectively. Those in 2015 were 59.9 ±13.3 cm, 38.0 ±11.1 cm, and 31.2 ±11.7 cm, respectively. The snow depth on larch/shrub was significantly deeper than that on other vegetation in each year ($p<0.05$). The snow density on larch/shrub, sedge/sphagnum, and river/lake in 2014 were 0.194 ±0.028 g/cm^3, 0.185 ±0.030 g/cm^3, and 0.277 ±0.042 g/cm^3, respectively. Those in 2015 were 0.186 ±0.019 g/cm^3, 0.172 ±0.031 g/cm^3, and 0.227 ±0.044 g/cm^3, respectively. The snow density on river/lake was significantly higher than that on other vegetation in each year ($p<0.05$). The SWE on larch/shrub, sedge/sphagnum, and river/lake in 2014 were 135.3 ±35.5 mm, 84.1 ±13.0 mm, and 113.8 ±31.0 mm, respectively. Those in 2015 were 112.9 ±31.7 mm, 66.2 ±27.1 mm, and 72.7 ±31.7 mm, respectively. The SWE on larch/shrub was significantly higher than that on sedge/sphagnum in 2014 and that on other vegetation in 2015 ($p<0.05$). The $\delta^{18}O$ of snow cover on larch/shrub, sedge/sphagnum, and river/lake in 2014 were −30.8 ±1.9‰, −29.8 ±1.2‰, and −28.9 ±3.2‰, respectively. Those in 2015 were −27.2 ±2.3‰, −28.1 ±1.6‰, and −26.9 ±2.4‰, respectively. There was no significant difference among the $\delta^{18}O$ of snow cover on each vegetation in both years.

4.4. Discussion

4.4.1. Metamorphism and re-distribution of snow

There seems to be no biased spatial distribution (locational difference) in snow cover within this study area scale, but spatial heterogeneity of the snow parameters depending on the vegetation was observed. The snow depth on larch/shrub was significantly deeper than that on the others, suggesting that re-distribution due to blowing snow occurred and the trees and shrubs branches caught the blowing snow. As a result, the snow depth on sedge/sphagnum with no trees which catch the snow became shallower. On the river/lake, there is no obstacles to prevent wind circumferentially, therefore it is considered that the snow depth was reduced and the snow density was increased due to compressed snow by strong wind. Since the SWE on larch/shrub was significantly higher than the others, the snow depth may contribute to the SWE more than the snow density.

4.4.2. Calculation of local Snow Water Equivalent

Since the snow cover data depends on the vegetation in the study area, the local scale SWE can be calculated by scaling up using a vegetation map. From the vegetation map and vegetation classification by Morozumi et al. (2019), the coverages of each vegetation type of 10 km × 10 km around site K were 39.4% for larch/shrub, 41.4% for sedge/sphagnum, and 19.8% for river/lake. The locale scale SWE for this study area was calculated from these percentages to be 111 mm in 2014 and 86 mm in 2015. Considering loss due to sublimation, which is 25-50% of total snowfall (e.g. Pomeroy et al., 1997;

Liston & Sturm, 1998; Essery et al., 1999), precipitation during winter (i.e., total snowfall) is predicted to be 149–224 mm in 2014 and 117–176 mm in 2015. These data are critically important for improving the accuracy of remote sensing and numerical models.

4.5. Summary

Snow survey was conducted to know the spatial variations in snow depth, density, SWE and stable isotopic composition in Indigirka River lowland near Chokurdakh (70.62 N, 147.90 E), Northeastern Siberia, and to estimate SWE in areal or reginal scale, by scaling-up based on topographic and vegetative controls on SWE.

The ranges of snow depth, density, SWE and $\delta^{18}O$ in this area observed in 2014 were 30 to 90 cm, 0.137 to 0.318 g/cm^3, 70 to 200 mm and −36.5 to −22.9‰, respectively, whereas those observed in 2015 were 12 to 83 cm, 0.131 to 0.325 g/cm^3, 20 to 160 mm and −31.2 to −22.8‰, respectively. Although the values and the ranges were slightly different between 2014 and 2015, observed snow cover properties depended on vegetation type and showed consistencies: snow cover was the deepest at the site covered by dense and tall shrub, while snow density was the highest on ice over a lake. The SWE was the highest at shrub site, whereas that was the lowest at the site of sedge and/or sphagnum wetland. Since clear relationship between SWE and vegetation type, we estimated regional SWE in observation area (10 × 10 km) using a vegetation map. The values were 111 mm in 2014 and 86 mm in 2015.

Table 4.1. Summary of observed data at each sampling point.

Sampling point	Sampling date	Latitude	Longitude	Elevation (m)	Snow depth (cm)	Snow density (g/cm^3)	Snow water equivalent (mm)	δD (‰)	$\delta^{18}O$ (‰)	d-excess (‰)	Land cover classification
CV1	23 April 2014	70° 34'12.54"N	147° 52'16.44"E	8	37	0.227	83.4	-221	-28.8	9	sedge / sphagnum
CV2	23 April 2014	70° 32'9.96"N	147° 52'12.48"E	11	73	0.183	133.5	-231	-30.6	13	larch / shrub
CV3	23 April 2014	70° 31'27.3"N	147° 77'27.72"E	13	76	0.227	172.4	-275	-36.5	17	larch / shrub
CV4	23 April 2014	70° 28'13.2"N	147° 40'55.44"E	8	72	0.185	132.7	-234	-30.9	12	larch / shrub
CV5	23 April 2014	70° 24'13.62"N	147° 33'14.34"E	6	80	0.235	187.3	-244	-32.2	14	larch / shrub
CV6	23 April 2014	70° 20'55.14"N	147° 33'26.76"E	11	60	0.162	97.5	-236	-31.0	12	larch / shrub
CV7	23 April 2014	70° 15'2.52"N	147° 28'14.1"E	8	62	0.193	119.6	-224	-29.4	11	larch / shrub
CA1	24 April 2014	70° 35'4.98"N	147° 45'53.88"E	7	49	0.203	100.0	-222	-29.2	12	sedge / sphagnum
CA2	24 April 2014	70° 32'48.48"N	147° 34'3.96"E	9	45	0.185	82.8	-229	-30.4	14	sedge / sphagnum
CA3	24 April 2014	70° 29'46.98"N	147° 25'35.82"E	8	63	0.170	106.6	-214	-28.2	11	larch / shrub
CA4	24 April 2014	70° 26'21.12"N	147° 18'20.64"E	7	58	0.186	108.7	-243	-32.7	18	larch / shrub
K1	25 April 2014	70° 33'48.78"N	148° 16'20.34"E	5	50	0.175	87.3	-209	-28.2	16	sedge / sphagnum
K2	25 April 2014	70° 33'45"N	148° 16'30.66"E	7	80	0.190	152.0	-227	-30.1	14	larch / shrub
K3	25 April 2014	70° 33'41.34"N	148° 16'43.08"E	1	82	0.196	161.0	-228	-30.4	16	larch / shrub
K4	25 April 2014	70° 33'37.98"N	148° 17'0.84"E	6	85	0.255	216.9	-215	-28.5	13	larch / shrub
K5	25 April 2014	70° 33'37.5"N	148° 17'29.16"E	10	67	0.190	127.3	-221	-29.5	15	larch / shrub
K6	25 April 2014	70° 33'35.04"N	148° 17'50.58"E	10	54	0.166	89.8	-231	-30.9	16	sedge / sphagnum
K7	25 April 2014	70° 33'32.88"N	148° 18'12.96"E	5	65	0.144	93.5	-232	-30.9	15	sedge / sphagnum
K8	26 April 2014	70° 33'48.84"N	148° 15'52.08"E	8	50	0.139	69.6	-218	-29.0	14	sedge / sphagnum
K9	26 April 2014	70° 33'47.64"N	148° 15'52.38"E	7	60	0.192	115.2	-234	-31.0	14	larch / shrub
K10	26 April 2014	70° 33'47.1"N	148° 15'52.98"E	9	67	0.204	136.4	-227	-30.2	15	larch / shrub
K11	26 April 2014	70° 33'44.7"N	148° 16'3.36"E	12	57	0.137	77.8	-230	-30.2	12	larch / shrub
K12	26 April 2014	70° 33'42.72"N	148° 16'18.9"E	13	58	0.206	119.2	-224	-29.6	13	larch / shrub
K13	26 April 2014	70° 33'37.5"N	148° 16'36.48"E	13	40	0.178	71.1	-217	-28.5	11	sedge / sphagnum
K14	26 April 2014	70° 33'31.08"N	148° 17'0.48"E	11	40	0.254	101.8	-216	-27.6	5	river / lake
K15	26 April 2014	70° 33'28.74"N	148° 17'22.98"E	8	32	0.318	101.7	-211	-27.1	6	river / lake
K16	26 April 2014	70° 33'23.94"N	148° 17'42.6"E	9	47	0.170	79.7	-213	-28.7	17	sedge / sphagnum
K17	26 April 2014	70° 33'19.32"N	148° 17'57.18"E	8	37	0.186	68.7	-223	-29.8	15	sedge / sphagnum
K18	26 April 2014	70° 33'18.72"N	148° 18'8.76"E	11	45	0.194	87.1	-226	-29.9	13	sedge / sphagnum
K19	26 April 2014	70° 33'27.06"N	148° 18'6.3"E	7	37	0.193	71.3	-225	-29.6	11	sedge / sphagnum
K20	26 April 2014	70° 33'33.54"N	148° 17'39.96"E	11	48	0.216	103.6	-231	-30.7	14	sedge / sphagnum
K21	26 April 2014	70° 33'33.42"N	148° 17'13.5"E	9	52	0.307	159.7	-248	-32.9	15	river / lake
K22	26 April 2014	70° 33'34.62"N	148° 16'51.66"E	7	40	0.230	91.8	-200	-25.5	4	river / lake
K23	26 April 2014	70° 33'38.46"N	148° 16'26.82"E	8	40	0.154	61.5	-217	-28.7	13	sedge / sphagnum
K24	26 April 2014	70° 33'41.82"N	148° 16'7.98"E	10	41	0.251	103.1	-247	-33.0	16	sedge / sphagnum
K25	26 April 2014	70° 33'44.22"N	148° 15'57.66"E	10	50	0.188	93.8	-216	-28.9	15	sedge / sphagnum
K26	15 April 2015	70° 33'48.36"N	148° 16'9.78"E	4	78	0.290	158.9	-214	-28.6	15	larch / shrub
K27	15 April 2015	70° 33'43.74"N	148° 16'8.22"E	4	50	0.158	79.1	-187	-25.4	15	larch / shrub
K28	15 April 2015	70° 33'38.4"N	148° 16'6"E	5	45	0.183	59.0	-207	-27.9	15	sedge / sphagnum
K29	15 April 2015	70° 33'35.58"N	148° 16'19.62"E	2	65	0.178	115.8	-205	-27.5	15	larch / shrub
K30	15 April 2015	70° 33'38.88"N	148° 16'31.14"E	3	53	0.205	108.7	-199	-26.4	12	sedge / sphagnum
K31	15 April 2015	70° 33'41.34"N	148° 16'44.04"E	7	32	0.172	54.9	-172	-23.2	14	larch / shrub
K32	15 April 2015	70° 33'36.78"N	148° 17'6.24"E	7	57	0.174	99.1	-214	-28.6	15	larch / shrub
K33	15 April 2015	70° 33'31.62"N	148° 16'54.66"E	1	35	0.294	102.9	-233	-29.7	5	river / lake
K34	15 April 2015	70° 33'26.76"N	148° 16'49.92"E	6	32	0.232	74.1	-194	-25.4	9	river / lake
K35	16 April 2015	70° 33'46.8"N	148° 15'56.22"E	6	63	0.204	128.4	-218	-29.1	15	larch / shrub
K36	16 April 2015	70° 33'46.32"N	148° 15'51.12"E	5	25	0.179	44.8	-216	-29.0	16	sedge / sphagnum
K37	16 April 2015	70° 33'48"N	148° 15'46.68"E	2	40	0.240	96.1	-226	-29.3	9	river / lake
K38	16 April 2015	70° 33'49.86"N	148° 15'47.7"E	1	45	0.191	85.7	-212	-27.9	11	river / lake
K39	16 April 2015	70° 33'48.3"N	148° 15'51.3"E	5	30	0.138	41.4	-210	-28.3	16	sedge / sphagnum
K40	16 April 2015	70° 33'35.28"N	148° 17'22.74"E	1	43	0.159	68.5	-175	-23.9	16	larch / shrub
K41	16 April 2015	70° 33'27.18"N	148° 17'9.72"E	1	37	0.325	120.1	-217	-28.2	8	river / lake
K42	16 April 2015	70° 33'24.42"N	148° 17'18.06"E	1	32	0.266	85.2	-230	-29.8	8	river / lake
K43	16 April 2015	70° 33'29.88"N	148° 17'31.2"E	1	30	0.177	53.1	-237	-31.2	12	sedge / sphagnum
K44	16 April 2015	70° 33'26.1"N	148° 17'54.12"E	3	44	0.179	78.6	-186	-24.9	13	larch / shrub
K45	16 April 2015	70° 33'27"N	148° 18'1.68"E	-1	48	0.211	101.4	-178	-24.9	22	river / lake
K46	16 April 2015	70° 33'29.82"N	148° 18'2.82"E	-4	22	0.202	44.3	-205	-27.1	13	river / lake
K47	16 April 2015	70° 33'37.14"N	148° 18'15.42"E	5	57	0.176	100.3	-197	-26.5	15	larch / shrub
K48	16 April 2015	70° 33'37.56"N	148° 18'17.58"E	13	72	0.225	161.8	-183	-24.8	15	larch / shrub
K49	16 April 2015	70° 33'30.96"N	148° 17'38.64"E	7	45	0.200	90.2	-207	-27.9	16	sedge / sphagnum
CV8	17 April 2015	70° 36'38.1"N	147° 51'31.86"E	-7	13	0.206	26.8	-198	-24.2	-5	river / lake
CV9	17 April 2015	70° 36'39.66"N	147° 51'28.74"E	-2	55	0.211	115.9	-194	-26.0	14	larch / shrub
CV10	17 April 2015	70° 32'26.28"N	147° 52'39.42"E	4	55	0.178	97.8	-221	-29.7	17	larch / shrub
CV11	17 April 2015	70° 31'38.46"N	147° 48'27.72"E	-4	12	0.171	20.5	-199	-24.7	-2	river / lake
CV12	17 April 2015	70° 29'9.18"N	147° 41'14.94"E	-1	22	0.192	42.2	-195	-24.2	-1	river / lake
CV13	17 April 2015	70° 29'9.72"N	147° 41'12"E	1	58	0.198	115.0	-180	-23.6	9	larch / shrub
CV14	17 April 2015	70° 24'7.38"N	147° 32'55.92"E	-5	83	0.195	162.0	-235	-30.7	11	larch / shrub
CV15	17 April 2015	70° 20'56.46"N	147° 33'30.54"E	3	43	0.210	90.4	-172	-22.8	10	river / lake
CV16	17 April 2015	70° 20'56.4"N	147° 33'27.78"E	5	70	0.187	130.6	-215	-28.5	12	larch / shrub
CV17	17 April 2015	70° 15'58.2"N	147° 27'34.14"E	-6	25	0.219	54.6	-197	-24.7	1	river / lake
CV18	17 April 2015	70° 16'0.12"N	147° 27'38.46"E	5	63	0.200	126.1	-216	-28.7	14	larch / shrub
CV19	17 April 2015	70° 15'2.4"N	147° 28'10.26"E	2	73	0.172	125.9	-208	-27.4	11	larch / shrub

Table 4.2. Average values and standard deviation of snow parameters for each vegetation.

Year	Land cover classification	Snow depth (cm)	Snow density (g/cm^3)	SWE (mm)	$\delta^{18}O$ (‰)
2014	larch / shrub	68.7 ± 9.6	0.194 ± 0.028	135.3 ± 35.5	-30.8 ± 1.9
	sedge / sphagnum	45.9 ± 7.5	0.185 ± 0.030	84.1 ± 13.0	-29.8 ± 1.2
	river / lake	41.0 ± 8.2	0.277 ± 0.042	113.8 ± 31.0	-28.9 ± 3.2
2015	larch / shrub	59.9 ± 13.3	0.186 ± 0.019	112.9 ± 31.7	-27.2 ± 2.3
	sedge / sphagnum	38.0 ± 11.1	0.172 ± 0.031	66.2 ± 27.1	-28.1 ± 1.6
	river / lake	31.2 ± 11.7	0.227 ± 0.044	72.7 ± 31.7	-26.9 ± 2.4

(a)

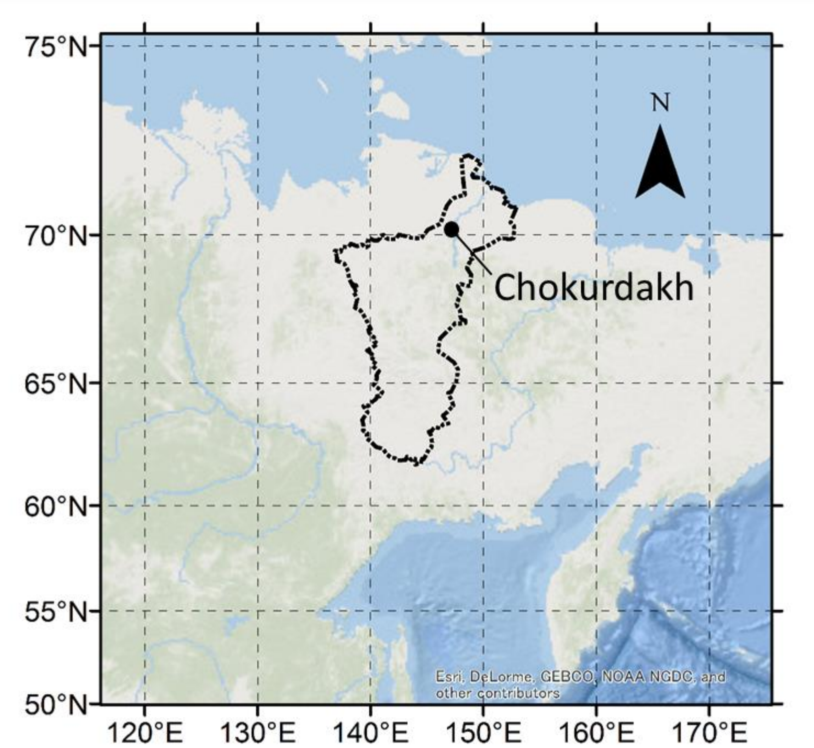
75°N
70°N
65°N
60°N
55°N
50°N
120°E
130°E
140°E
150°E
160°E
170°E
N
Chokurdakh
Esri, DeLorme, GEBCO, NOAA NGDC, and other contributors

(b)

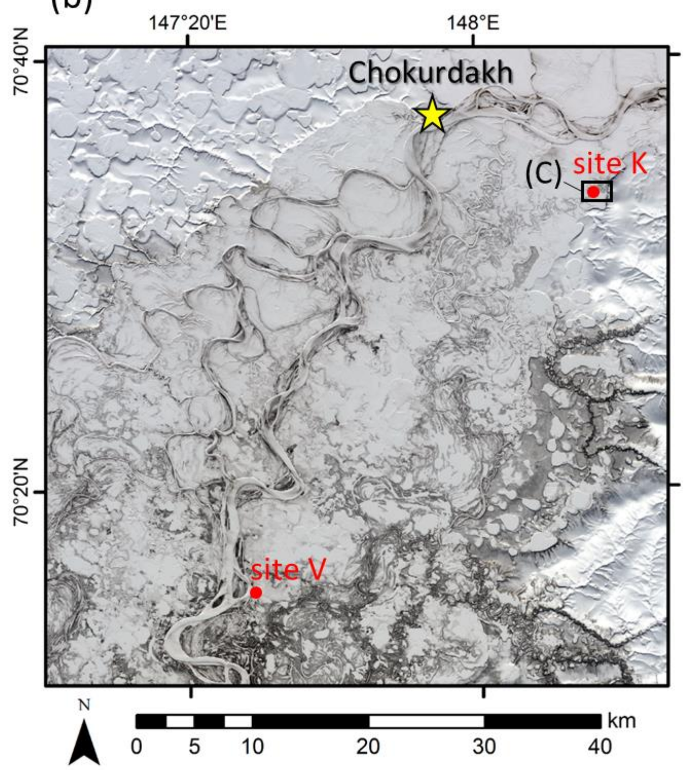
147°20'E
148°E
70°40'N
70°20'N
Chokurdakh
(C)
site K
site V
N
0
5
10
20
30
40
km

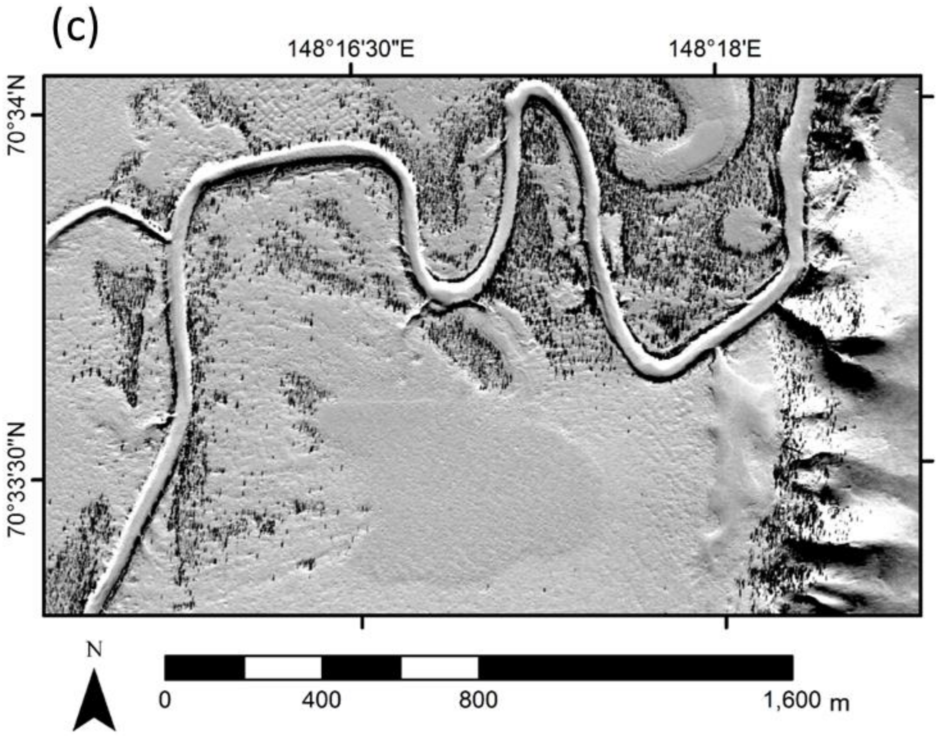

Figure 4.1. Locations of the observation area. (a) Location of the study area. The dashed line shows the watershed of the Indigirka River. (b) Satellite photo around Chokurdakh, Landsat 8 (17 April 2015). (c) Satellite photo at site K, World View 2 (3 April 2012).

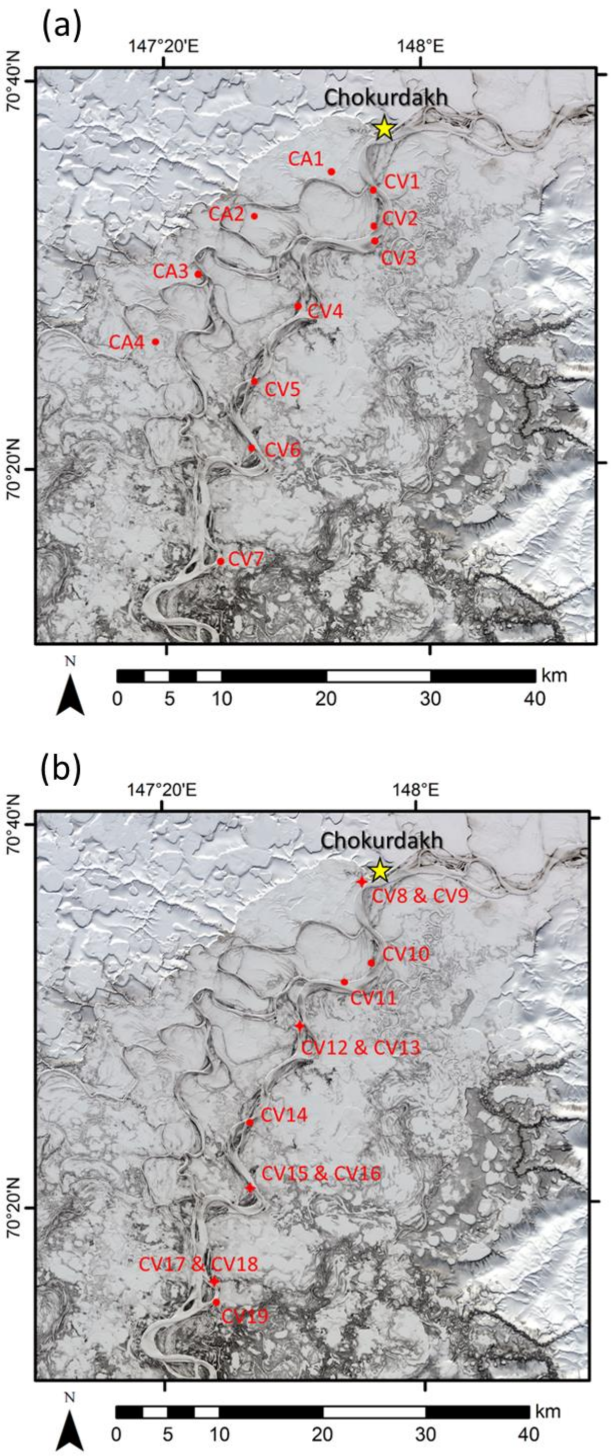

Figure 4.2. Sampling points around Chokurdakh in 2014 (a) and 2015 (b). At the Four-pointed star, observation was conducted at two points with different vegetation.

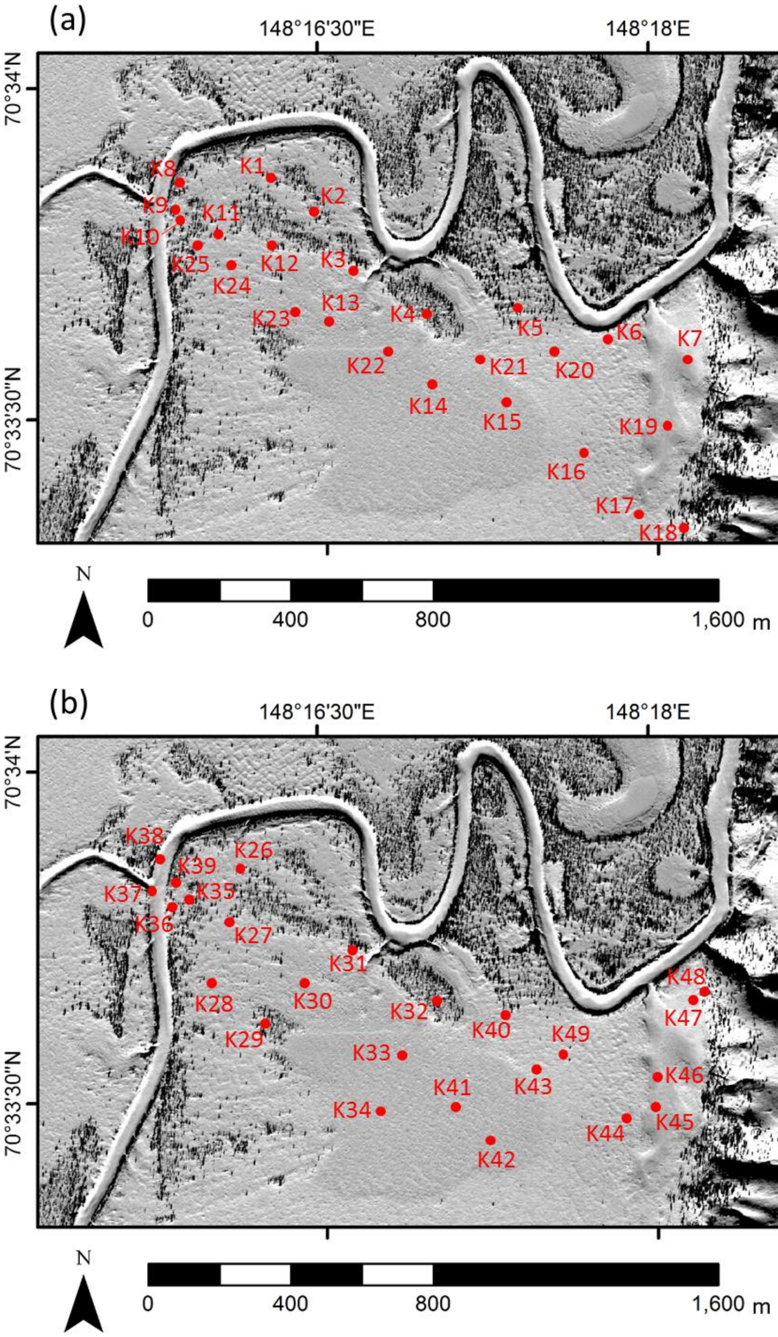

Figure 4.3. Sampling points at site K in 2014 (a) and 2015 (b).

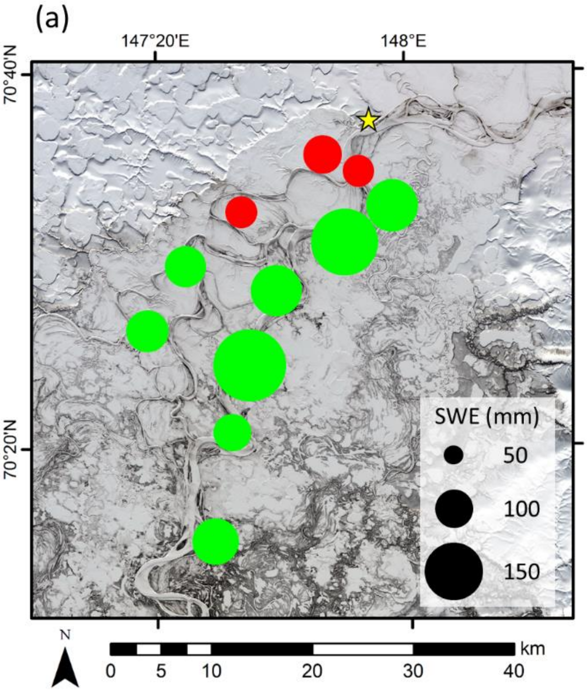
(a)
147°20'E
148°E
70°40'N
70°20'N
SWE (mm)
50
100
150
N
km
0
5
10
20
30
40

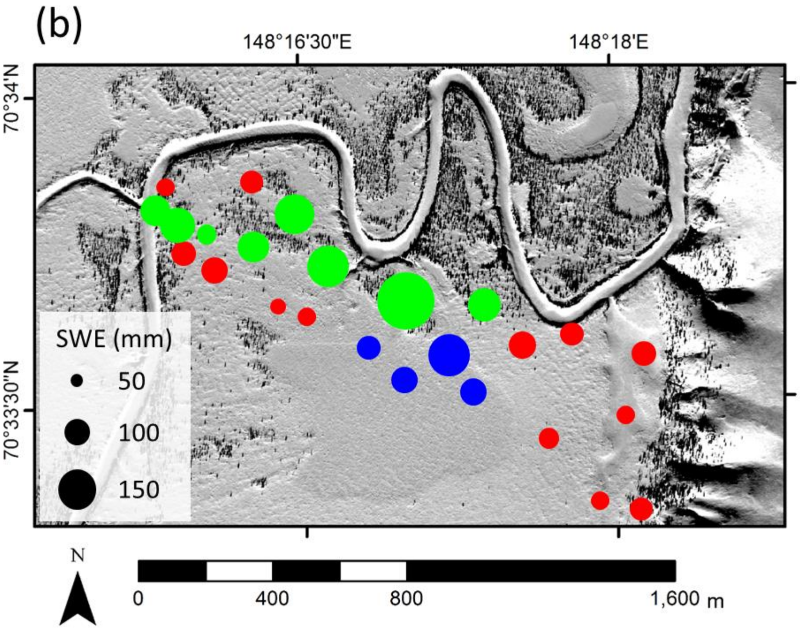
(b)
148°16'30"E
148°18'E
70°34'N
70°33'30"N
SWE (mm)
50
100
150
N
0
400
800
1,600
m

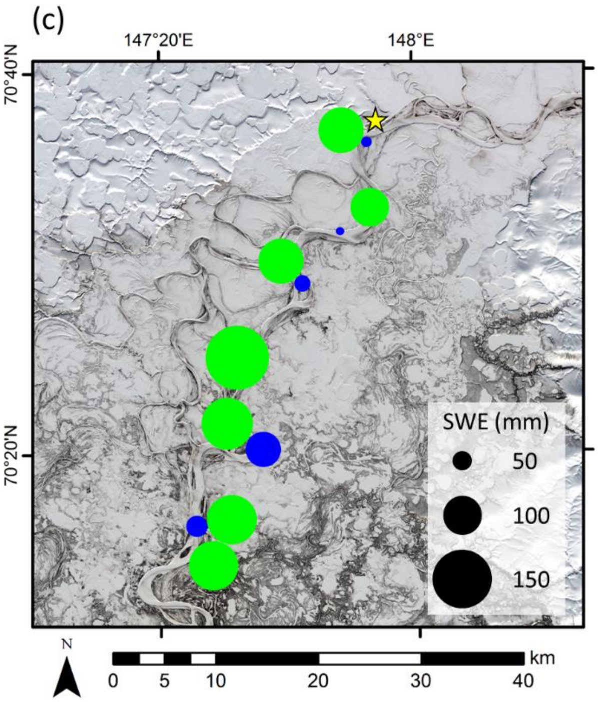

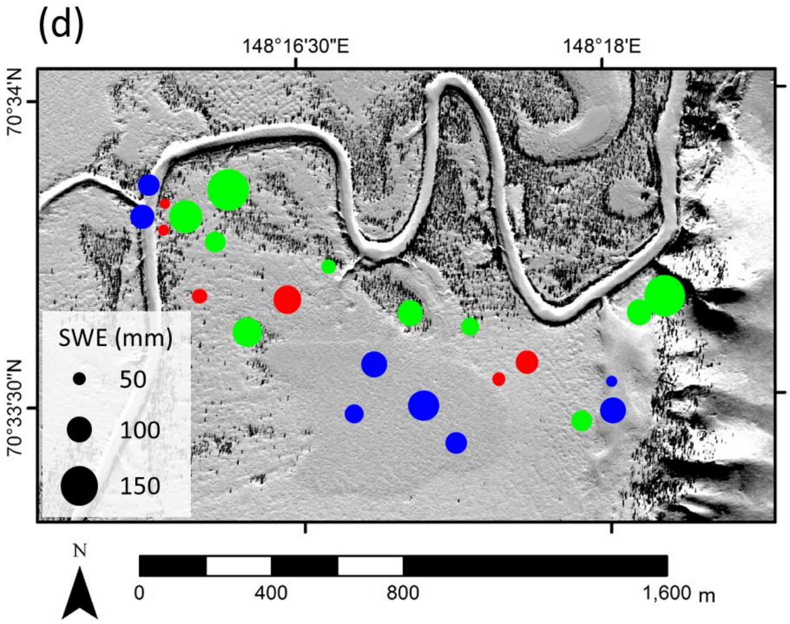

Figure 4.4. The Snow water equivalent (SWE) around Chokurdakh (a) and site K (b) in 2014, and the SWE around Chokurdakh (c) and site K (d) in 2015. The size of the circle indicates the SWE value at that point. Green, red, and blue circles shows the SWE on larch/shrub, sedge/sphagnum, and river/lake, respectively.

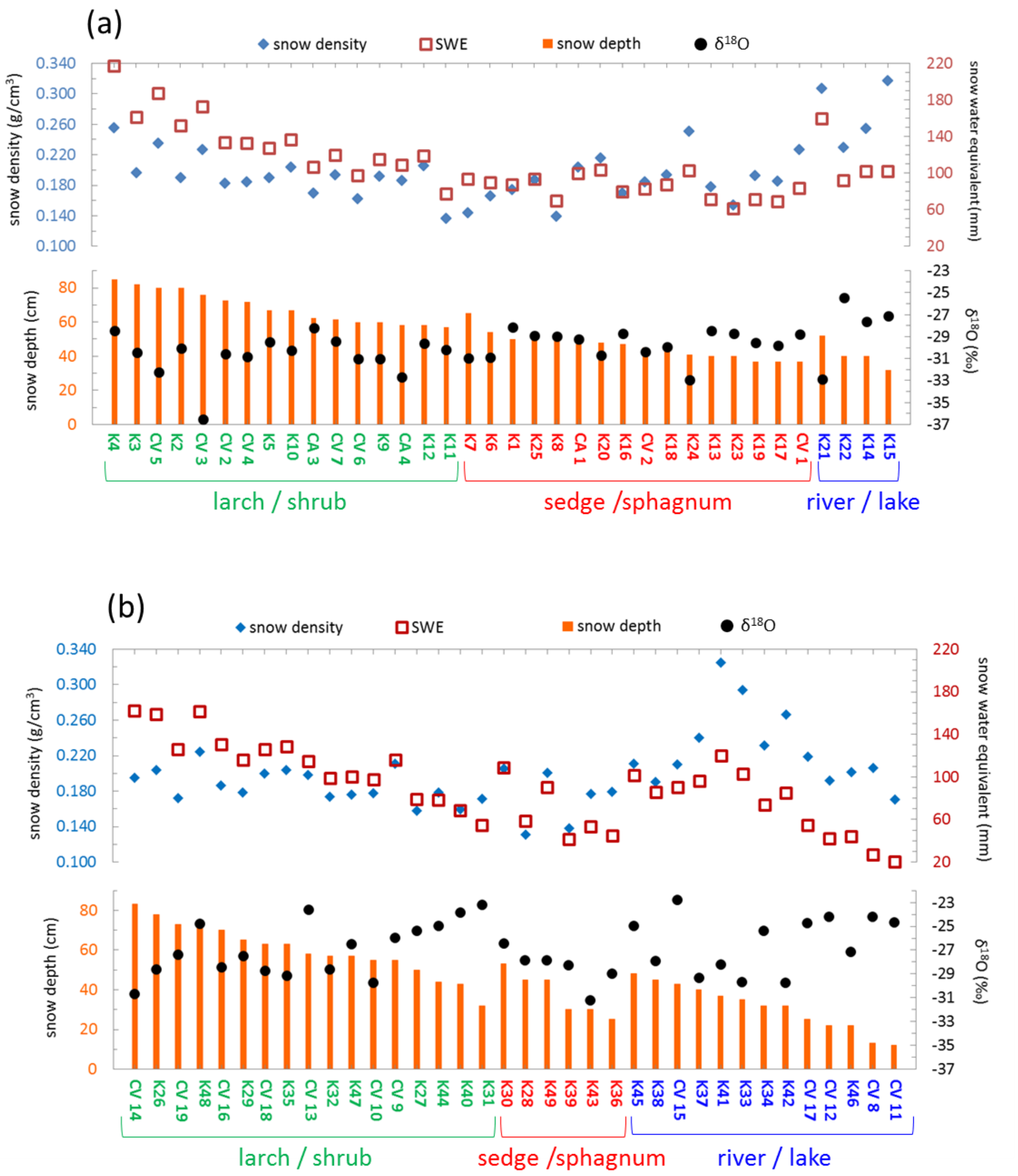

Figure 4.5. Snow density, SWE, snow depth, and $\delta^{18}O$ for each sampling point in 2014 (a) and 2015 (b).

Chapter 5. General discussion and Conclusions

5.1. General discussion

5.1.1. Relationship among ground ice, vegetation, microtopography and snow cover at the Taiga−Tundra boundary

The interaction between ground ice and ground surface conditions was observed at the Taiga–Tundra boundary in the Indigirka River lowlands, northeastern Siberia. It seems that the presence of ground ice formed microtopography which controls vegetation structure and composition at the Taiga−Tundra boundary, conversely, microtopography and vegetation affect the freezing environment of ground ice through such as soil moisture and shading effect. The microtopography and vegetation also controls the spatial distribution in snow cover at the study area, the snow cover affects the soil freezing environment such as ground temperature through the thermal conductivity. Therefore, the ground ice and the ground surface conditions affect one another.

At the tree mounds, lower soil moisture with higher relative elevation due to ice-rich layer in the surface permafrost causes lower thermal conductivity in the surface soil. In addition, the presence of tree and shrub increases snow depth, which also causes the lower thermal conductivity. This lower thermal conductivity causes slow freezing of the ground in winter. It is considered that the environment where slow freezing occurs caused ice segregation in the ground, resulting in ice-rich condition. The permafrost thawing is disturbed through the shading effect during summer (Blok et al., 2010). In contrast at the wet areas, higher soil moisture with lower relative elevation due to ice-poor layer in the surface permafrost and shallower snow depth cause higher thermal conductivity in the surface soil, which causes rapid freezing of the ground in winter. It is considered that the environment where rapid freezing occurs was hard to form segregation ices in the ground, resulting in ice-poor condition. The permafrost thawing is more progressive than at the tree mounds during summer due to the high thermal conductivity.

5.1.2. Future changes in permafrost and ground surface conditions

At the Taiga–Tundra boundary of northeastern Siberia in the Arctic region, the predicted warming trend and the increases in snowfall and tree and shrub are expected to lead to an increase in ground temperature and permafrost thawing, causing microtopographic avalanches and subsidence. On the other hand, the increases in snow cover and tree and shrub cause slow freezing of the ground in winter, so the formation of ground ice may conversely cause the microtopographic heaving if there is a short-term cold period. These microtopographic changes can significantly impact the vegetation structure and composition at the Taiga–Tundra boundary ecosystem.

5.2. Conclusions

Future possible changes in snow cover, soil moisture, and organic soil, which also depend on the vegetation and microtopography, could have significant impacts on the freezing environment of the ground ice at the Taiga–Tundra boundary of northeastern Siberia in the Arctic region. These changes in the freezing environment may then in turn affect the vegetation through changes in the microtopography of the ground surface.

The results of this study should greatly contribute to research on permafrost degradation and associated vegetation and microtopography changes at the Taiga–Tundra boundary in northeastern Siberia. Future work will involve collecting data from other Taiga and Taiga–Tundra boundary areas and conducting experimental studies on soil freezing. Further investigations on vegetation and microtopography changes are necessary to predict permafrost degradation due to climate change.

Acknowledgements

I sincerely thank all the referees and staffs involved in the examination of this doctoral dissertation for the important opportunity and helpful comments.

I would like to express my deepest gratitude to Professor Atsuko Sugimoto of Hokkaido University for the precious opportunity of conducting this study, patient mentoring, and important supports for my research life.

I sincerely appreciate continued helpful advices and kind encouragements from Professor Masanobu Yamamoto, Associate Professor Yohei Yamashita and Assistant Professor Tomohisa Irino of Hokkaido University.

I sincerely thank Dr. Go Iwahana of Hokkaido University and University of Alaska Fairbanks for mentoring permafrost sampling, mentoring in the beginning of my fieldwork, and helpful advices about permafrost and physical environment.

I sincerely appreciate the supports for my fieldwork in the vicinity of Chokurdakh given by Dr. Trofim Maximov, Dr. Alexander Kononov, Mr. Roman Petrov, Mr. Egor Starostin, Dr. Stanislav Ksenofontov, Ms. Alexandra Alexeeva, and other members of the Institute for Biological Problems of Cryolithozone (IBPC), Siberian Branch of the Russian Academy of Sciences, and Ms. Tatiana Stryukova, Mr. Sergey Ianygin, and other staffs at the Allikhovsky Ulus Inspectorate of Nature Protection.

I also would like to appreciate technical and secretarial supports in Sugimoto Laboratory from Ms. Yumi Hoshino, Ms. Satori Nunohashi, Ms. Kanako Tanaka, Ms. Kayoko Saito, Ms. Hanae Kudo, and Dr. Masanori Ito. I truly thank Dr. Shunsuke Tei, Dr. Maochang Liang, Dr. Ryo Shingubara, and Dr. Tomoki Morozumi in the lab for collecting a part of the physical data, helpful information about the studied ecosystem, and valuable cooperation in relation to their researches about forest ecology, isotope ecology, CH_4 flux, and vegetation and remote sensing of the study area, respectively. I also wish to express my appreciation to Dr. Ivan Bragin, Dr. Yumiko Miyamoto, Dr. Akihiro Ueta, Dr. Alexandra Popova, Dr. Lei Fujiyoshi, Dr. Xiaoyang Li, Dr. Fang Li, Mr. Yohei Chiba, Ms. Megumi Nakamura, Ms. Asami Kitayama, Mr. Shinichi Tanabe, Dr. Rong Fan, Mr. Ruslan Shakhmatov, Ms. Hikari Shimada, Mr. Soma Saito, Mr. Atsuki Mori, Mr. Danfeng Zhou, Mr. Shuhei Hashiguchi, Mr. Shihong Zhong, Mr. Aleksandr Nogovitsyn, Mr. Kei Tanekura, and other previous and current members in Sugimoto Laboratory for helps with my fieldwork and research life.

Finally, I sincerely thank all the people who supported or encouraged this study.

Reference

Allison SD, Wallenstein MD, Bradford MA. Soil-carbon response to warming dependent on microbial physiology. Nat Geosci. 2010; 3(5): 336-340. https://doi.org/10.1038/ngeo846

Blok D, Heijmans M, Schaepman-Strub G, Kononov AV, Maximov TC, Berendse F. Shrub expansion may reduce summer permafrost thaw in Siberian tundra. Glob Chang Biol. 2010; 16(4): 1296-1305. https://doi.org/10.1111/j.1365-2486.2009.02110.x|

Boch MS. Bolota tundrovoi zony Sibiri (printsipy tipologii). In Tipy bolot SSSR i printsipy ikh klassifikatsii,Abramova TG (ed.). Akademiya Nauk SSSR: Leningrad. 1974; 146–154.

Boudreau LD, Rouse WR. THE ROLE OF INDIVIDUAL TERRAIN UNITS IN THE WATER-BALANCE OF WETLAND TUNDRA. Clim Res. 1995; 5(1): 31-47. https://doi.org/10.3354/cr005031

Bring A, Fedorova I, Dibike Y, Hinzman L, Mard J, Mernild SH, et al. Arctic terrestrial hydrology: A synthesis of processes, regional effects, and research challenges. J Geophys Res Biogeosci. 2016; 121(3): 621-649. https://doi.org/10.1002/2015JG003131

Brown RD, Mote PW. The Response of Northern Hemisphere Snow Cover to a Changing Climate. Journal of Climate. 2009; 22(8): 2124-45.

Burn CR, Kokelj SV. The environment and permafrost of the Mackenzie Delta area, Permafr Periglac Process. 2009; 20: 83-105. https://doi.org/10.1002/ppp.655

Callaghan TV, Johansson M, Brown RD, Groisman PY, Labba N, Radionov V, et al. The Changing Face of Arctic Snow Cover: A Synthesis of Observed and Projected Changes. Ambio. 2011; 40: 17-31. https://doi.org/10.1007/s13280-011-0212-y

Cheng G. The mechanism of repeated-segregation for the formation of thick-layered ground ice. Cold Reg Sci and Technol. 1983; 8: 57-66. https://doi.org/10.1016/0165-232X(83)90017-4

Chernov Y, Matveyeva N. Arctic ecosystems in Russia. In: Wielgolaski F (ed.). Ecosystems of the World. Amsterdam: Elsevier. 1997; 361–507.

Craig H, Gordon LI. Deuterium and oxygen 18 variations in the ocean and the marine atmosphere. In: Tongiorgi E (ed.). Stable Isotopes in Oceanographic Studies and Paleotemperatures. Lab. di Geol. Necl., Pisa, Italy. 1965; 9–130.

Craig H. ISOTOPIC VARIATIONS IN METEORIC WATERS. Science. 1961; 133(346): 1702-1703. https://doi.org/10.1126/science.133.3465.1702

Dansgaard W. STABLE ISOTOPES IN PRECIPITATION. Tellus. 1964; 16(4): 436-468.

https://doi.org/10.3402/tellusa.v16i4.8993

Derksen C, Toose P, Rees A, Wang L, English M, Walker A, et al. Development of a tundra-specific snow water equivalent retrieval algorithm for satellite passive microwave data. Remote Sensing of Environment. 2010; 114(8): 1699-709.

Elberling B. Annual soil CO2 effluxes in the High Arctic: The role of snow thickness and vegetation type. Soil Biology & Biochemistry. 2007; 39(2): 646-54.

Engstrom R, Hope A, Kwon H, Stow D, Zamolodchikov D. Spatial distribution of near surface soil moisture and its relationship to microtopography in the Alaskan Arctic coastal plain. Nordic Hydrology. 2005; 36(3): 219-234. https://doi.org/10.2166/nh.2005.0016

Essery R, Li L, Pomeroy J. A distributed model of blowing snow over complex terrain. Hydrological Processes. 1999; 13(14-15): 2423-38.

Essery R, Pomeroy J. Vegetation and topographic control of wind-blown snow distributions in distributed and aggregated simulations for an Arctic tundra basin. J Hydrometeorol. 2004; 5(5): 735-744. https://doi.org/10.1175/1525-7541(2004)005<0735:VATCOW>2.0.CO;2

Fan R, Morozumi T, Maximov TC, Sugimoto A. Effect of floods on the delta C-13 values in plant leaves: a study of willows in Northeastern Siberia. PeerJ. 2018; 6.

https://doi.org/10.7717/peerj.5374

French H, Shur Y. The principles of cryostratigraphy. Earth-Sci Rev. 2010; 101(3-4): 190-206. https://doi.org/10.1016/j.earscirev.2010.04.002

Fritz M, Wetterich S, Meyer H, Schirrmeister L, Lantuit H, Pollard WH. Origin and Characteristics of Massive Ground Ice on Herschel Island (Western Canadian Arctic) as revealed by Stable Water Isotope and Hydrochemical Signatures. Permafr Periglac Process. 2011; 22(1): 26-38. https://doi.org/10.1002/ppp.714

Fritz M, Wetterich S, Schirrmeister L, Meyer H, Lantuit H, Preusser F, et al. Eastern Beringia and beyond: Late Wisconsinan and Holocene landscape dynamics along the Yukon Coastal Plain, Canada. Palaeogeogr Palaeoclimatol Palaeoecol. 2012; 319: 28-45. https://doi.org/10.1016/j.palaeo.2011.12.015

Frost GV, Epstein HE. Tall shrub and tree expansion in Siberian tundra ecotones since the 1960s. Glob Change Biol. 2014; 20(4): 1264-1277. https://doi.org/10.1111/gcb.12406

Godin E, Fortier D, Levesque E. Nonlinear thermal and moisture response of ice-wedge polygons to permafrost disturbance increases heterogeneity of high Arctic wetland. Biogeosciences. 2016; 13(5): 1439-1452. https://doi.org/10.5194/bg-13-1439-2016

Hinzman LD, Kane DL, Gieck RE, Everett KR. HYDROLOGIC AND THERMAL-PROPERTIES OF THE ACTIVE LAYER IN THE ALASKAN ARCTIC. Cold Reg Sci Technol. 1991; 19(2): 95-110. https://doi.org/10.1016/0165-232X(91)90001-W

Hirashima H, Ohata T, Kodama Y, Yabuki H, Sato N, Georgiadi A. Nonuniform distribution of tundra snow cover in eastern Siberia. J Hydrometeorol. 2004; 5(3): 373-389. https://doi.org/10.1175/1525-7541(2004)005<0373:NDOTSC>2.0.CO;2

Ise T, Dunn AL, Wofsy SC, Moorcroft PR. High sensitivity of peat decomposition to climate change through water-table feedback. Nat Geosci. 2008; 1(11): 763-766. https://doi.org/10.1038/ngeo331

Iwahana G, Takano S, Petrov RE, Tei S, Shingubara R, Maximov TC, et al. Geocryological characteristics of the upper permafrost in a tundra-forest transition of the Indigirka River Valley, Russia. Polar Sci. 2014; 8(2): 96-113. https://doi.org/10.1016/j.polar.2014.01.005

Jorgenson MT, Racine CH, Walters JC, Osterkamp TE. Permafrost degradation and ecological changes associated with a warming climate in central Alaska. Clim Change. 2001; 48(4): 551-579. https://doi.org/10.1023/A:1005667424292

Kendall C, McDonnell JJ (eds.). Isotope Tracers in Catchment Hydrology. Amsterdam: Elsevier. 1998.

Khitun OV, Koroleva TM, Chinenko SV, Petrovsky VV, Pospelova EB, Pospelov IN, et al. Applications of local floras for floristic subdivision and monitoring vascular plant diversity in the Russian Arctic. Arct Sci. 2016; 2: 103-126. https://doi.org/10.1139/as-2015-0010

Kokelj SV, Burn CR, Tarnocai C. The structure and dynamics of earth hummocks in the subarctic forest near Inuvik, Northwest Territories, Canada. Arct Antarct Alp Res. 2007; 39: 99-109. https://doi.org/10.1657/1523-0430(2007)39[99:TSADOE]2.0.CO;2

Kokelj SV, Burn CR. Ground ice and soluable cations in near-surface permafrost, Inuvik, Northwest Territories, Canada. Permafr Periglac Process. 2003; 14: 275-289. https://doi.org/10.1002/ppp.458

Kokelj SV, Burn CR. Near-surface ground ice in sediments of the Mackenzie Delta, Northwest Territories, Canada. Permafr Periglac Process. 2005; 16: 291-303. https://doi.org/10.1002/ppp.537

Koven CD, Ringeval B, Friedlingstein P, Ciais P, Cadule P, Khvorostyanov D, et al. Permafrost carbon-climate feedbacks accelerate global warming. Proc Nati Acad

Sci USA. 2011; 108(36): 14769-14774. https://doi.org/10.1073/pnas.1103910108

Kravtsova VI, Loshkareva AR. Dynamics of vegetation in the tundra-taiga ecotone on the Kola Peninsula depending on climate fluctuations. Russ J Ecol. 2013; 44(4): 303-311. https://doi.org/10.1134/S1067413613040085

Lacelle D, Fontaine M, Forest AP, Kokelj S. High-resolution stable water isotopes as tracers of thaw unconformities in permafrost: A case study from western Arctic Canada. Chem Geol. 2014; 368: 85-96. https://doi.org/10.1016/j.chemgeo.2014.01.005

Lacelle D. On the delta O-18, delta D and D-excess Relations in Meteoric Precipitation and During Equilibrium Freezing: Theoretical Approach and Field Examples. Permafr Periglac Process. 2011; 22(1): 13-25. https://doi.org/10.1002/ppp.712

Lachniet MS, Lawson DE, Sloat AR. Revised C-14 dating of ice wedge growth in interior Alaska (USA) to MIS 2 reveals cold paleoclimate and carbon recycling in ancient permafrost terrain. Quat Res. 2012; 78(2): 217-225. https://doi.org/10.1016/j.yqres.2012.05.007

Larsen KS, Grogan P, Jonasson S, Michelsen A. Respiration and Microbial Dynamics in Two Subarctic Ecosystems during Winter and Spring Thaw: Effects of Increased Snow Depth. Arctic Antarctic and Alpine Research. 2007; 39(2): 268-76.

Lawrence DM, Slater AG, Swenson SC. Simulation of Present-Day and Future Permafrost and Seasonally Frozen Ground Conditions in CCSM4. J Clim. 2012; 25(7): 2207-2225. https://doi.org/10.1175/JCLI-D-11-00334.1

Lemke P, Ren J, Alley RB, Allison I, Carrasco J, Flato G, et al. Observations: changes in snow, ice and frozen ground. In: Solomon S, Qin D, Manning M, Chen Z, Marquis M, Averyt KB, et al. (eds.), Climate Change 2007: the Physical Science Basis. Contribution of Working Group I to the Fourth Assessment Report of the Intergovernmental Panel on Climate Change, Cambridge University Press, Cambridge, United Kingdom and New York, NY, USA. 2007; 337-383.

Liang MC, Sugimoto A, Tei S, Bragin IV, Takano S, Morozumi T, et al. Importance of soil moisture and N availability to larch growth and distribution in the Arctic taiga-tundra boundary ecosystem, northeastern Siberia. Polar Sci. 2014; 8(4): 327-341. https://doi.org/10.1016/j.polar.2014.07.008

Ling F, Zhang TJ. Modeled impacts of changes in tundra snow thickness on ground thermal regime and heat flow to the atmosphere in Northernmost Alaska. Global and Planetary Change. 2007; 57(3-4): 235-46.

Liston GE, Sturm M. A snow-transport model for complex terrain. Journal of Glaciology. 1998; 44(148): 498-516.

Mackay JR. Oxygen isotope variations in permafrost, Tuktoyaktuk Peninsula area, Northwest Territories. Curr Res Part B, Geol Surv Can. 1983; Paper 83–1B; 67-74.

Matsumoto J, Ohkubo T. Experimental study on heat transfer characteristics of soils. Proceedings of the Japan society of civil engineers. 1977; 257: 43-50. https://doi.org/10.2208/jscej1969.1977.53

McGuire AD, Anderson LG, Christensen TR, Dallimore S, Guo LD, Hayes DJ, et al. Sensitivity of the carbon cycle in the Arctic to climate change. Ecol Monogr. 2009; 79(4): 523-555. https://doi.org/10.1890/08-2025.1

Merlivat L, Jouzel J. GLOBAL CLIMATIC INTERPRETATION OF THE DEUTERIUM-OXYGEN-18 RELATIONSHIP FOR PRECIPITATION. J Geophys Res Oceans. 1979; 84(NC8): 5029-5033. https://doi.org/10.1029/JC084iC08p05029

Meyer H, Dereviagin A, Siegert C, Hubberten HW. Palaeoclimate studies on Bykovsky Peninsula, North Siberia - hydrogen and oxygen isotopes in ground ice. Polarforschung. 2002a; 70: 37-51.

Meyer H, Dereviagin A, Siegert C, Schirrmeister L, Hubberten HW. Palaeoclimate reconstruction on Big Lyakhovsky Island, North Siberia - Hydrogen and oxygen isotopes in ice wedges. Permafr Periglac Process. 2002b; 13(2): 91-105. https://doi.org/10.1002/ppp.416

Meyer H, Opel T, Laepple T, Dereviagin AY, Hoffmann K, Werner M. Long-term winter warming trend in the Siberian Arctic during the mid-to late Holocene. Nat Geosci. 2015; 8(2): 122-125. https://doi.org/10.1038/ngeo2349

Meyer H, Schirrmeister L, Yoshikawa K, Opel T, Wetterich S, Hubberten HW, et al. Permafrost evidence for severe winter cooling during the Younger Dryas in northern Alaska. Geophys Res Lett. 2010; 37. https://doi.org/10.1029/2009GL041013

Michel FA. Isotope Characterisation of Ground Ice in Northern Canada. Permafr Periglac Process. 2011; 22(1): 3-12. https://doi.org/10.1002/ppp.721

Minke M, Donner N, Karpov N, de Klerk P, Joosten H. Patterns in Vegetation Composition, Surface Height and Thaw Depth in Polygon Mires in the Yakutian Arctic (NE Siberia): A Microtopographical Characterisation of the Active Layer. Permafr Periglac Process. 2009; 20(4): 357-368. https://doi.org/10.1002/ppp.663

Minke M, Donner N, Karpov NS, de Klerk P, Joosten H. Distribution, diversity, development and dynamics of polygon mires: examples from NE Yakutia (NE Siberia). Peatlands Int. 2007; 1: 36–40.

Morozumi T, Shingubara R, Suzuki R, Kobayashi H, Tei S, Takano S, et al. Estimating methane emissions using 1 vegetation mapping in the taiga-tundra boundary of a north-eastern Siberian lowland. Tellus B Chem Phys Meteorol. 2019; 71(1): 1-17. https://doi.org/10.1080/16000889.2019.1581004

Morse PD, Burn CR. Field observations of syngenetic ice wedge polygons, outer Mackenzie Delta, western Arctic coast, Canada. J Geophys Res Earth Surf. 2013; 118: 1320-1332. https://doi.org/10.1002/jgrf.20086

O'Neil JR. HYDROGEN AND OXYGEN ISOTOPE FRACTIONATION BETWEEN ICE AND WATER. J Phys Chem. 1968; 72(10): 3683-3684. https://doi.org/10.1021/j100856a060

Opel T, Dereviagin AY, Meyer H, Schirrmeister L, Wetterich S. Palaeoclimatic Information from Stable Water Isotopes of Holocene Ice Wedges on the Dmitrii Laptev Strait, Northeast Siberia, Russia. Permafr Periglac Process. 2011; 22(1): 84-100. https://doi.org/10.1002/ppp.667

Opel T, Laepple T, Meyer H, Dereviagin AY, Wetterich S. Northeast Siberian ice wedges confirm Arctic winter warming over the past two millennia. Holocene. 2017; 27(11): 1789-1796. https://doi.org/10.1177/0959683617702229

Park H, Sherstiukov AB, Fedorov AN, Polyakov IV, Walsh JE. An observation-based assessment of the influences of air temperature and snow depth on soil temperature in Russia. Environmental Research Letters. 2014; 9(6).

Pomeroy JW, Essery RLH. Turbulent fluxes during blowing snow: field tests of model sublimation predictions. Hydrological Processes. 1999; 13(18): 2963-75.

Pomeroy JW, Marsh P, Gray DM. Application of a distributed blowing snow model to the arctic. Hydrological Processes. 1997; 11(11): 1451-64.

Pomeroy JW, Parviainen J, Hedstrom N, Gray DM. Coupled modelling of forest snow interception and sublimation. Hydrological Processes. 1998; 12(15): 2317-37.

Porter TJ, Froese DG, Feakins SJ, Bindeman IN, Mahony ME, Pautler BG, et al. Multiple water isotope proxy reconstruction of extremely low last glacial temperatures in Eastern Beringia (Western Arctic). Quat Sci Rev. 2016; 137: 113-125. https://doi.org/10.1016/j.quascirev.2016.02.006

Raisanen J. Warmer climate: less or more snow? Clim Dyn. 2008; 30(2-3): 307-319. https://doi.org/10.1007/s00382-007-0289-y

Ranson KJ, Montesano PM, Nelson R. Object-based mapping of the circumpolar taiga-tundra ecotone with MODIS tree cover. Remote Sens Environ. 2011; 115(12): 3670-3680. https://doi.org/10.1016/j.rse.2011.09.006

Rees A, English M, Derksen C, Toose P, Silis A. Observations of late winter Canadian tundra snow cover properties. Hydrological Processes. 2014; 28(12): 3962-77.

Romanovsky VE, Drozdov DS, Oberman NG, Malkova GV, Kholodov AL, Marchenko SS, et al. Thermal State of Permafrost in Russia. Permafr Periglac Process. 2010; 21(2): 136-155. https://doi.org/10.1002/ppp.683

Romanovsky VE, Sazonova TS, Balobaev VT, Shender NI, Sergueev DO. Past and recent changes in air and permafrost temperatures in eastern Siberia. Glob Planet Change. 2007; 56(3-4): 399-413. https://doi.org/10.1016/j.gloplacha.2006.07.022

Schirrmeister L, Meyer H, Andreev A, Wetterich S, Kienast F, Bobrov A, et al. Late Quaternary paleoenvironmental records from the Chatanika River valley near Fairbanks (Alaska). Quat Sci Rev. 2016; 147: 259-278. https://doi.org/10.1016/j.quascirev.2016.02.009

Serreze MC, Barry RG. Processes and impacts of Arctic amplification: A research synthesis. Glob Planet Change. 2011; 77(1-2): 85-96. https://doi.org/10.1016/j.gloplacha.2011.03.004

Shingubara R, Sugimoto A, Murase J, Iwahana G, Tei S, Liang MC, et al. Multi-year effect of wetting on CH4 flux at taiga-tundra boundary in northeastern Siberia deduced from stable isotope ratios of CH4. Biogeosciences. 2019; 16(3): 755-768. https://doi.org/10.5194/bg-16-755-2019

Shur Y, Hinkel KM, Nelson FE. The transient layer: Implications for geocryology and climate-change science. Permafr Periglac Process. 2005; 16(1): 5-17. https://doi.org/10.1002/ppp.518

Sidorchuk AY, Panin AV, Borisova OK, Elias SA, Syvistki JP. Channel morphology and river flow in the northern Russian Plain in the Late Glacial and Holocene. Int J Earth Sci. 2000; 89: 541-549. https://doi.org/10.1007/s005310000132

Souchez RA, Jouzel J. ON THE ISOTOPIC COMPOSITION IN DELTA-D AND DELTA-O-18 OF WATER AND ICE DURING FREEZING. J Glaciol. 1984; 30(106): 369-372. https://doi.org/10.3189/S0022143000006249

Stow DA, Hope A, McGuire D, Verbyla D, Gamon J, Huemmrich F, et al. Remote sensing of vegetation and land-cover change in Arctic Tundra Ecosystems. Remote Sensing of Environment. 2004; 89(3): 281-308.

Streletskaya ID, Vasiliev AA, Oblogov GE, Tokarev IV. Reconstruction of paleoclimate of Russian arctic in Late Pleistocene-Holocene on the basis of isotope study of ice wedges. Earth's Cryosphere. 2015; 19(2): 98–106.

Stuiver M, Yang IC, Denton GH. PERMAFROST OXYGEN ISOTOPE RATIOS AND CHRONOLOGY OF 3 CORES FROM ANTARCTICA. Nature. 1976; 261(5561): 547-550. https://doi.org/10.1038/261547a0

Suzuoki T, Kjmura T. D/H and $^{18}O/^{16}O$ fractionation in ice-water system. J Mass Spectrom Soc Jpn. 1973; 21: 229–233. https://doi.org/10.5702/massspec1953.21.229

Tchebakova NM, Parfenova E, Soja AJ. The effects of climate, permafrost and fire on vegetation change in Siberia in a changing climate. Environ Res Lett. 2009; 4(4). http://dx.doi.org/10.1088/1748-9326/4/4/045013

Tei S, Sugimoto A, Liang M, Yonenobu H, Matsuura Y, Oosawa A, et al. Radial growth and physiological response of coniferous trees to Arctic amplification. J. Geophys. Res. 2017; 122: 2786-2803. https://doi.org/10.1002/2016JG003745

Tei S, Sugimoto A, Yonenobu H, Matsuura Y, Osawa A, Sato H, et al. Tree-ring analysis and modeling approaches yield contrary response of circumboreal forest productivity to climate change. Glob Chang Biol. 2017; 23(12): 5179-5188. https://doi.org/10.1111/gcb.13780

Tei S, Sugimoto A. Time lag and negative responses of forest greenness and tree growth to warming over circumboreal forests. Glob Chang Biol. 2018; 24(9): 4225-4237. https://doi.org/10.1111/gcb.14135

Vaganov E, Hughes MK, Kirdyanov AV, Schweingruber FH, Silkin PP. Influence of snowfall and melt timing on tree growth in subarctic Eurasia. Nature. 1999; 400:

149-151. https://doi.org/10.1038/22087

Van Everdingen R (ed.). Multi-language Glossary of Permafrost and Related Ground-ice Terms. National Snow and Ice Data Center/World Data Center for Glaciology, Boulder. 1998 (Rev. May 2005).

Vasil'chuk Y, Vasil'chuk A. Spatial distribution of mean winter air temperatures in Siberian permafrost at 20-18ka BP using oxygen isotope data. Boreas. 2014; 43(3): 678-687. https://doi.org/10.1111/bor.12033

Wetterich S, Rudaya N, Tumskoy V, Andreev AA, Opel T, Schirrmeister L, et al. Last Glacial Maximum records in permafrost of the East Siberian Arctic. Quat Sci Rev. 2011; 30(21-22): 3139-3151. https://doi.org/10.1016/j.quascirev.2011.07.020

Wetterich S, Tumskoy V, Rudaya N, Andreev AA, Opel T, Meyer H, et al. Ice Complex formation in arctic East Siberia during the MIS3 Interstadial. Quat Sci Rev. 2014; 84: 39-55. https://doi.org/10.1016/j.quascirev.2013.11.009

Wetterich S, Tumskoy V, Rudaya N, Kuznetsov V, Maksimov F, Opel T, et al. Ice Complex permafrost of MIS5 age in the Dmitry Laptev Strait coastal region (East Siberian Arctic). Quat Sci Rev. 2016; 147: 298-311. https://doi.org/10.1016/j.quascirev.2015.11.016

Wolter J, Lantuit H, Fritz M, Macias-Fauria M, Myers-Smith I, Herzschuh U. Vegetation composition and shrub extent on the Yukon coast, Canada, are strongly linked to ice-wedge polygon degradation. Polar Res. 2016; 35. http://dx.doi.org/10.3402/polar.v35.27489

Yabuki H, Park H, Kawamoto H, Suzuki R, Razuvaev VN, Bulygina ON, Ohata T. Baseline Meteorological Data in Siberia (BMDS) Version 5.0. RIGC, JAMSTEC, Yokosuka, Japan, distributed by CrDAP, Digital Media. 2011.

Yoshikawa K, Lawson D, Sharkhuu N. Stable isotope composition of ice core in open- and closed-system pingos. K.M. Hinkel (Ed.), Permafrost, Tenth International Conference, Proceedings, Salekhard, vol. 1, The Northern Publisher, Russia. 2012; 473-478.

Yoshikawa K, Natsagdorj S, Sharkhuu A. Groundwater Hydrology and Stable Isotope Analysis of an Open-System Pingo in Northwestern Mongolia. Permafr Periglac Process. 2013; 24(3): 175-183. https://doi.org/10.1002/ppp.1773

Zhang T, Barry RG, Knowles K, Ling F, Armstrong RL. Distribution of seasonally and perennially frozen ground in the Northern Hemisphere. Permafrost. 2003; 1289–1294.

Zhang TJ. Influence of the seasonal snow cover on the ground thermal regime: An overview. Rev Geophys. 2005; 43(4). https://doi.org/10.1029/2004RG000157

Zibulski R, Herzschuh U, Pestryakova LA. Vegetation patterns along micro-relief and vegetation type transects in polygonal landscapes of the Siberian Arctic. J Veg Sci. 2016; 27(2): 377-386. https://doi.org/10.1111/jvs.12356